Fluid-Rock Interaction and Hydrocarbon Migration: Quantifying Wettability-Affected Advection and Diffusion Processes in Various Reservoir Rocks*

Qinhong Hu[1]

Search and Discovery Article #42437 (2019)**
Posted December 16, 2019

*Adapted from oral presentation given at 2019 AAPG Annual Convention and Exhibition, San Antonio, Texas, May 19-22, 2019
**Datapages © 2019 Serial rights given by author. For all other rights contact author directly. DOI:10.1306/42437Hu2019

[1]The University of Texas at Arlington, Arlington, Texas (maxhu@uta.edu)

Abstract

Darcy-type advection is the dominant transport mechanism in sandstone and carbonate reservoirs, while diffusion (driven by concentration gradient) can be the main process to transport hydrocarbons inside low-permeable shale matrices. These advection and diffusion processes affect fluid flow and hydrocarbon migration, with their rates difficult to quantify in rocks with μm to nm-scaled pore networks. Microscopic characteristics of porous materials - pore shape, pore-size distribution, pore connectivity - influence macroscopic behavior of fluid flow and hydrocarbon migration. The pore structure (both geometry and topology) effect is further complicated by fluid-wet characteristics of reservoir rocks. Using custom-designed tracer recipes in hydrophilic, hydrophobic and zwittering fluids, followed with micro-scale mapping of laser ablation-inductively coupled plasma-mass spectrometry, this work presents experimental approaches to quantifying the rates of advection and diffusion in different reservoir types (sandstone, carbonate, and shale).

Results show that reservoir rock possesses a range of pore structure (with a wide range of pore sizes at μm to nm ranges, as well as different connectivity) to control the behavior and rates of imbibition and diffusion processes. Chemical diffusion in sparsely-connected pore spaces is not well described by classical Fickian behavior; anomalous behavior is suggested by percolation theory, and confirmed by results of our imbibition tests. Imbibition into a fluid-wet rock with well-connected pore spaces leads to mass uptake proportional to time, while sparsely-connected pores exhibit an imbibition exponent of 1/4, with a much lower rate and anomalous behavior. Overall findings for organic-rich shale indicate that the pore connectivity and “Dalmatian” wettability of organic and inorganic compositions are implicated with the entanglement of nano-sized molecules in ~5-10 nm-sized pore spaces.

Selected References

David, C., J. Wassermann, F. Amann, J. Klaver, C. Davy, J. Sarout, L. Esteban, E.H. Rutter, Q. Hu, L. Louis, P. Delage, D.A. Lockner, A.P.S. Selvadurai, T. Vanorio, A. Amann-Hildenbrand, P.G. Meredith, J. Browning, T.M. Mitchell, C. Madonna, J. Billiotte, T. Reuschlé, D. Lasseux,

J. Fortin, R. Lenormand, D. Loggia, F. Nono, G. Boitnott, E. Jahns, M. Fleury, G. Berthe, P. Braun, D. Grégoire, L. Perrier, P. Polito, Y. Jannot, A. Sommier, B. Krooss, R. Fink, and A. Clark, 2018, KG²B, A Collaborative Benchmarking Exercise for Estimating the Permeability of the Grimsel Granodiorite - Part 2: Modelling, Microstructures, and Complementary Data: Geophysical Journal International, v. 215/2, p. 825-843. doi.org/10.1093/gji/ggy305

Hu, Q., H. Liu, R. Yang, Y.X. Zhang, G. Kibria, S. Sahi, N. Alatrash, F.M. MacDonnell, and W. Chen, 2017, Applying Molecular and Nanoparticle Tracers to Study Wettability and Connectivity of Longmaxi Formation in Southern China: Journal of Nanoscience and Nanotechnology, v. 17, p. 6284-6295.

Hu, Q., T.J. Kneafsey, R.C. Trautz, and J.S.Y. Wang, 2002, Tracer Penetration into Welded Tuff Matrix from Flowing Fractures: Vadose Zone Journal, v. 1, p. 102-112.

Hu, Q., R.P. Ewing, and S. Dultz, 2012, Pore Connectivity in Natural Rock: Journal of Contaminant Hydrology, v. 133, p. 76-83. doi:10.1016/j.jconhyd.2012.03.006

Hu, Q., R.P. Ewing, and H.D. Rowe, 2015, Low Nanopore Connectivity Limits Gas Production in Barnett Formation: Journal of Geophysical Research – Solid Earth, v. 120/12, p. 8073-8087.

Hu, Q.H., W. Zhou, P. Huggins, and W.L. Chen, 2018, Pore Structure and Fluid Uptake of the Goddard Shale Formation in Southeastern Oklahoma, USA: Geofluids, Article ID 5381735.

Sun, M., B. Yu, Q. Hu, R. Yang, Y. Zhang, B. Li, Y.B. Melnichenko, and G. Cheng, 2017, Pore Structure Characterization of Organic-Rich Niutitang Shale from China: Small Angle Neutron Scattering (SANS) Study: International Journal of Coal Geology, v. 186, p. 115-125. dio:10.1016/j.coal.2017.12.006

Sun, M., B. Yu, Q. Hu, Y. Zhang, B. Li, R. Yang, Y.B. Melnichenko, and G. Cheng, 2017, Pore Characteristics of Longmaxi Shale Gas Reservoir in the Northwest of Guizhou, China: Investigations Using Small-Angle Neutron Scattering (SANS), Helium Pycnometry, and Gas Sorption Isotherm: International Journal of Coal Geology, v. 171, p. 61-68.

Walls, J., A. Morcote, T. Hintzman, and M. Everts, 2016, Comparative Core Analysis from a Wolfcamp Formation Well; A Case Study: International Symposium of the Society of Core Analysts held in Snow Mass, Colorado, USA, 21-26 August 2016, SCA2016-044, 6 p.

Yang, R., S. He, Q. Hu, M. Sun, D. Hu, and J. Yi, 2017, Applying SANS Technique to Characterize Nano-Scale Pore Structure of Longmaxi Shale, Sichuan Basin (China): Fuel, v. 197, p. 91-99.

Zhang, Y.X., T.J. Barber, Q.H. Hu, M.K. Bleuel, and H.F. El-Sobky. 2019, Complementary Neutron Scattering, Mercury Intrusion and SEM Imaging Approaches to Micro- and Nano-pore Structure Characterization of Tight Rocks: A case study of the Bakken shale: International Journal of Coal Geology, v. 212, p. 103252

Zhao, J.H., Z.J. Jin, Q.H. Hu, Z.K. Jin, T.J. Barber, Y.X. Zhang, and M.K. Bleuel, 2017, Integrating SANS and Fluid-Invasion Methods to Characterize Pore Structure of Typical American Shale Oil Reservoirs: Scientific Reports, v. 7, p. 15413.

AAPG ACE 2019 ANNUAL CONVENTION & EXHIBITION

UNIVERSITY OF TEXAS-ARLINGTON

Fluid-Rock Interaction and Hydrocarbon Migration: Quantifying Wettability-Affected Advection and Diffusion Processes in Various Reservoir Rocks

(Max) Qinhong Hu

maxhu@uta.edu

C3PM

Consortium for Collaborative Characterization of Porous Media

$\phi_a \chi \tau r k \mathcal{D}$

Del Rio, TX

Oil & Gas Production: From Reservoir to Source Rock

UNIVERSITY OF TEXAS-ARLINGTON

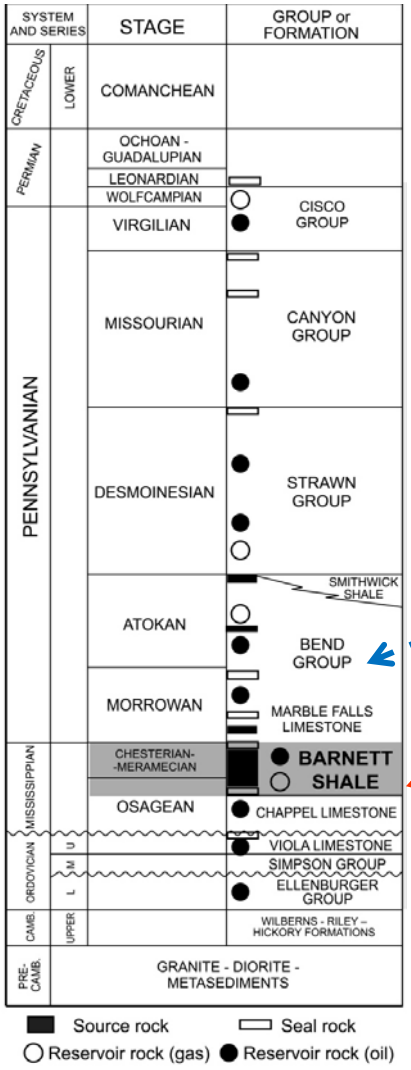

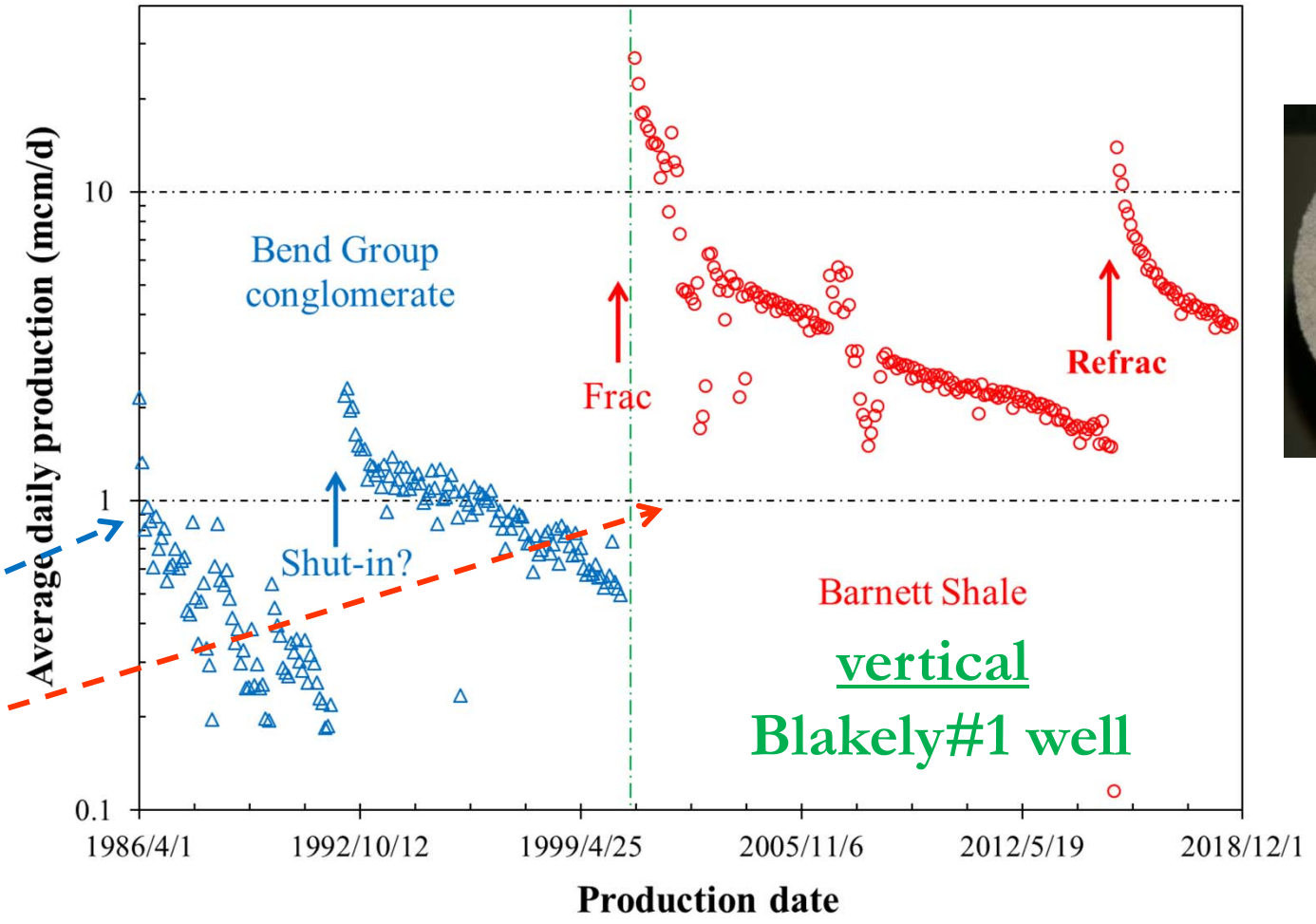

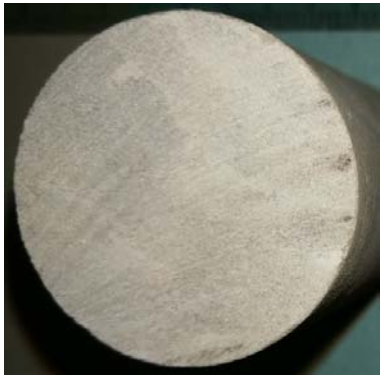

Pollastro (2003)

Petrophysics

UNIVERSITY OF TEXAS-ARLINGTON

- Petrophysics (*petro* is Latin for "rock" and *physics* is the study of nature)
- The study of rock and fluid (gas, liquid hydrocarbons, and aqueous solutions) properties as well as their interactions
- Milestones: Kozeny (1927); Schlumberger brothers (1936); Buckley and Leveret (1941); Archie (1942); 1947: Morse et al. (1947); Archie (1950; suggested the name of petrophysics); Welge (1952); Johnson et al. (1958); 1960s (peak days); …..

Nano-petrophysics: petrophysical studies in tight reservoirs with a predominant presence of nanopores

Different Rocks and Connectivity

UNIVERSITY OF TEXAS-ARLINGTON

Rock	Source	Porosity (%)	Permeability (m^2)
Berea Sandstone	Berea Quarry, OH	22.8	9.1×10^{-13}
Indiana Sandstone	Gas Storage Formation, IN	17.6	1.8×10^{-13}
Welded Tuff	Yucca Mtn., NV	9.25	5.0×10^{-19}
Meta-graywacke	The Geysers, CA	3.85	1.2×10^{-17}
Granite	Stripa mine, Sweden	0.4	$< 1 \times 10^{-19}$
Barnett shale	Wise Co., TX	2-5%	$\sim 5 \times 10^{-21}$

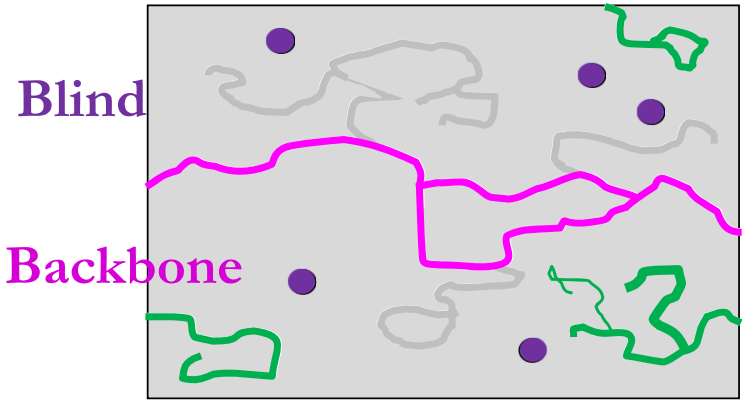

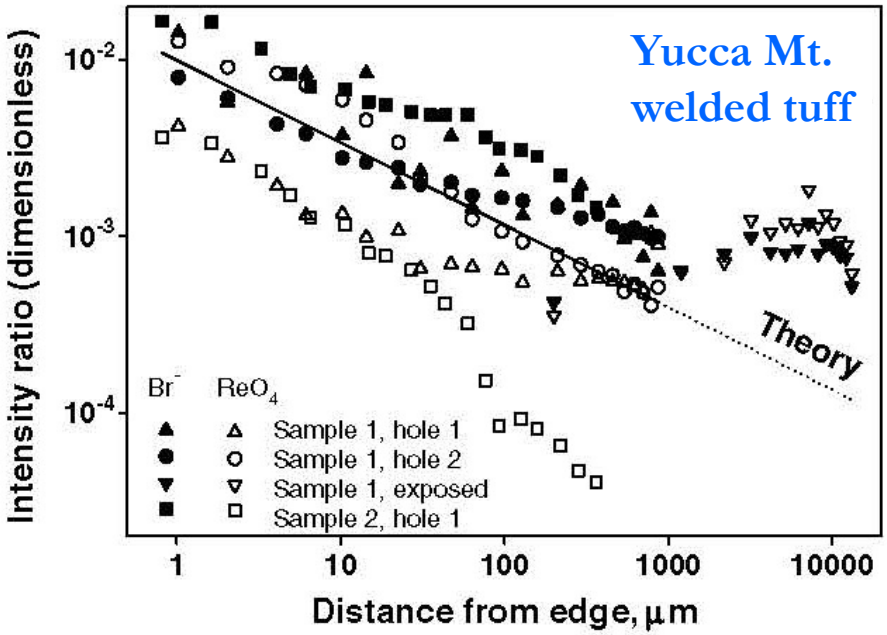

Hu et al., JCH, 2012

Edge-accessible Effective Porosity

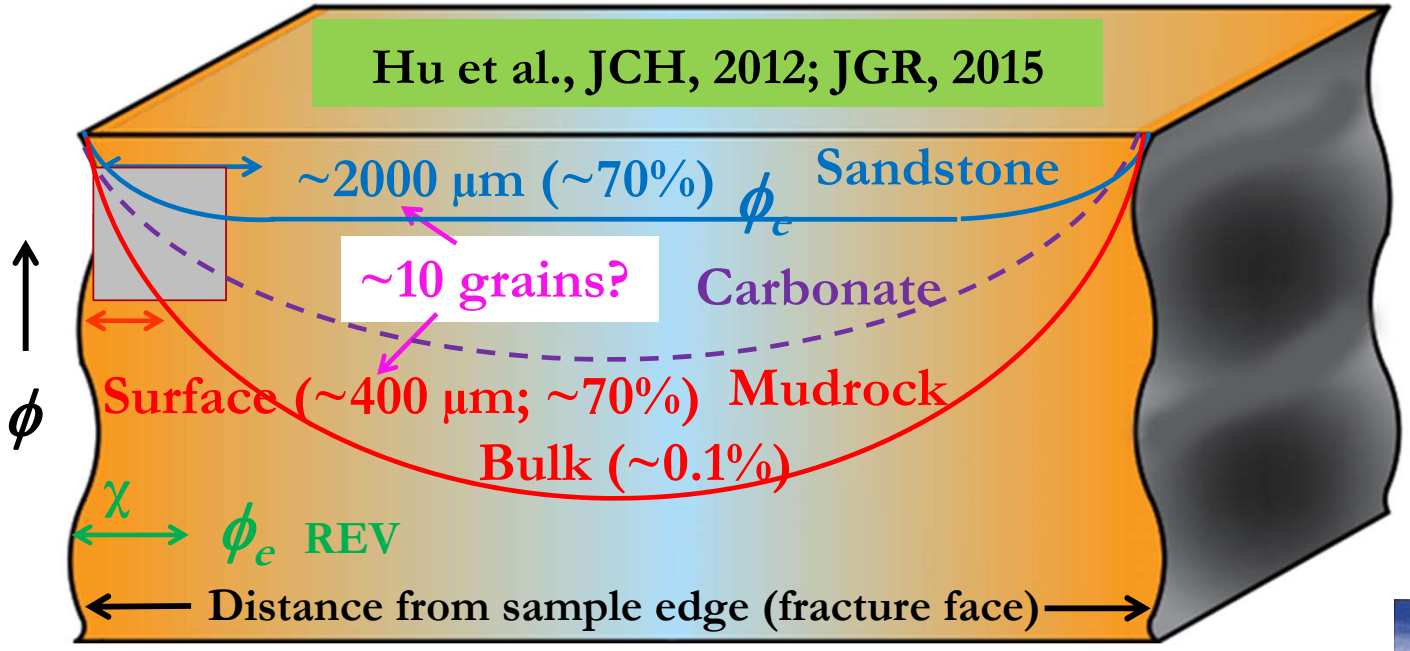

- Larger proportion of closed pores for larger sample sizes
- Assess pore connectivity by measuring effective porosity of different sample sizes

Up-scaling (percolation)

$$\phi(h) = \phi_e \begin{cases} (h/\chi)^{\beta/\nu} & h < \chi \\ 1 & h > \chi \end{cases}$$

χ: correlation length

β and υ: percolation exponents — 0.41 and 0.88 for 3-D

Pore Structure, Wettability, and Hydrocarbon Movement

UNIVERSITY OF TEXAS-ARLINGTON

Accessory data

- TOC
- Maturity
- Mineralogy
- Pyrolysis
- Well logging
- Production

✓ Gas and liquid pycnometry (different sample sizes)

✓ MIP (different sizes)

✓ Gas physisorption

✓ (U)SANS & SAXS

✓ NMR & NMRc

✓ GRI matrix k

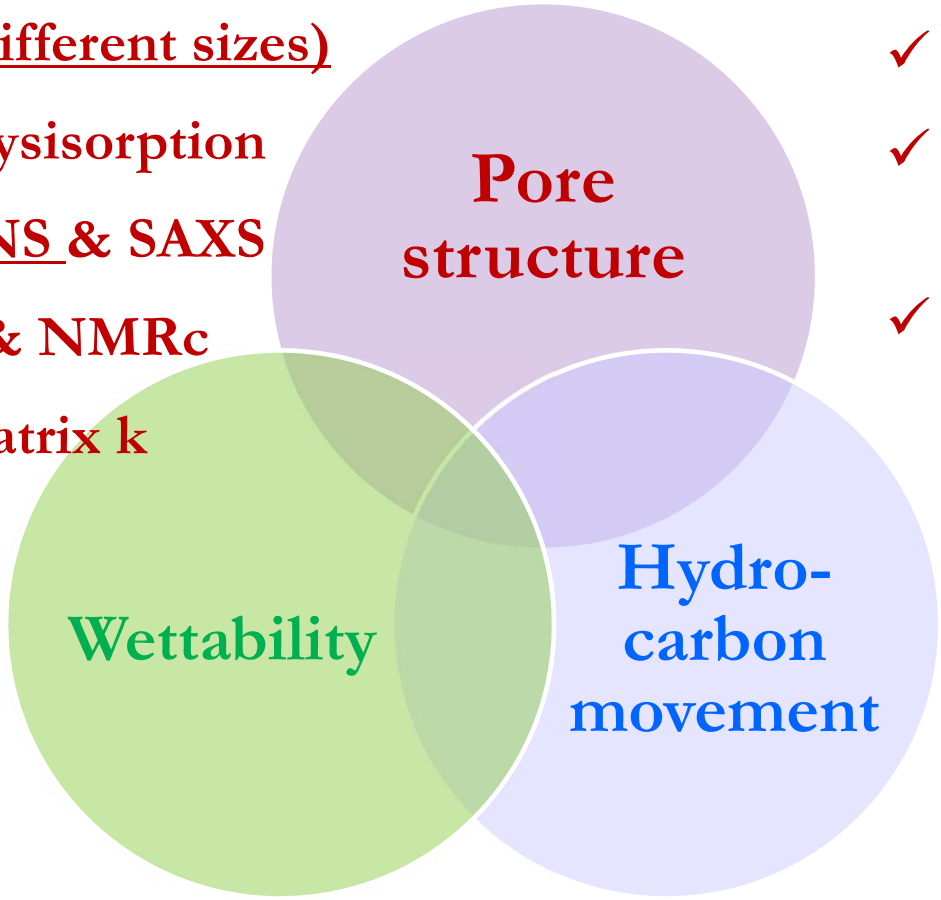

✓ FE-SEM & FIB-SEM

✓ CT

✓ Wood's metal

✓ Vacuum saturation for edge-accessible porosity

✓ Imbibition

✓ Wettability tracers

✓ Imbibition

✓ Diffusion

✓ NMR

✓ Core & dm-block flooding

✓ Contact angle

✓ Imbibition

✓ QEMSCAN for Dalmatian pattern

MIP Approach to Pore Structure Characterization

UNIVERSITY OF TEXAS-ARLINGTON

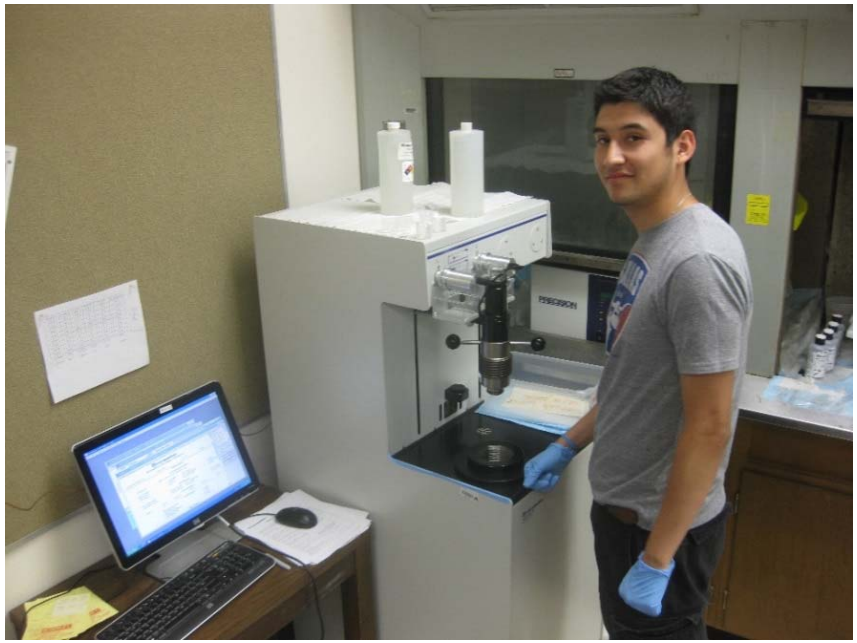

Barnett Shale sample (~15 mm cube) in the penetrometer

- Mercury Intrusion Porosimetry (MIP)
- Measurable pore diameter range: 3 nm to 360 µm

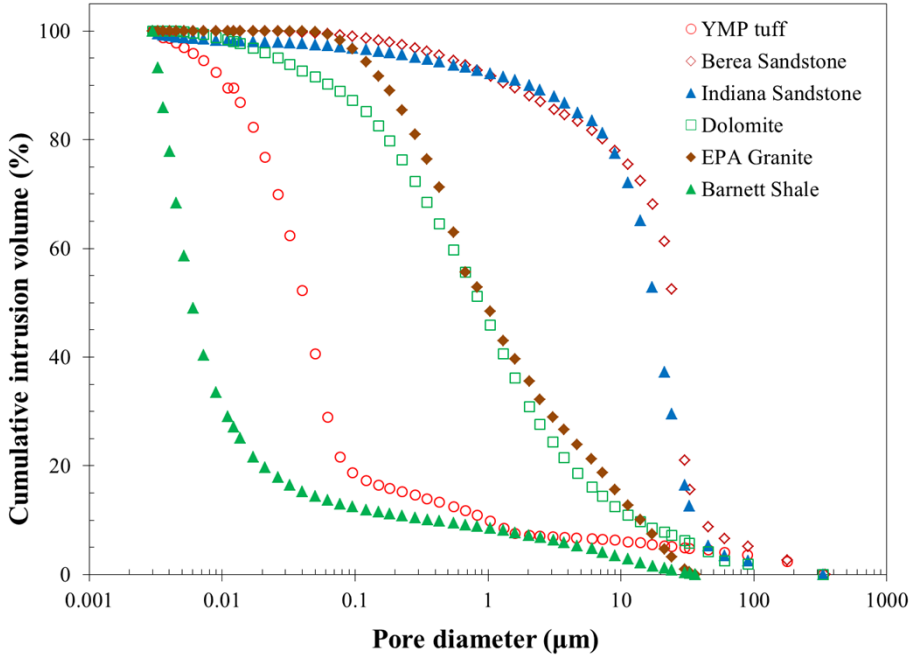

MIP: Conformance, Blank Correction, Validation, and Detection Limit

UNIVERSITY OF TEXAS-ARLINGTON

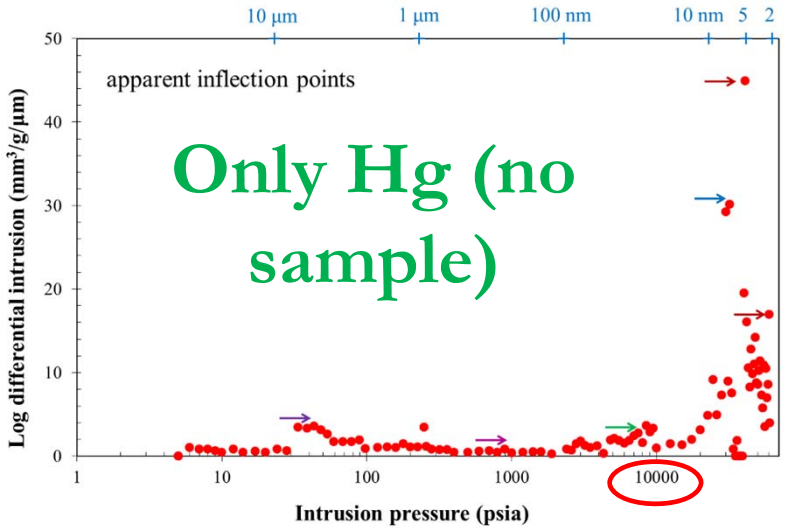

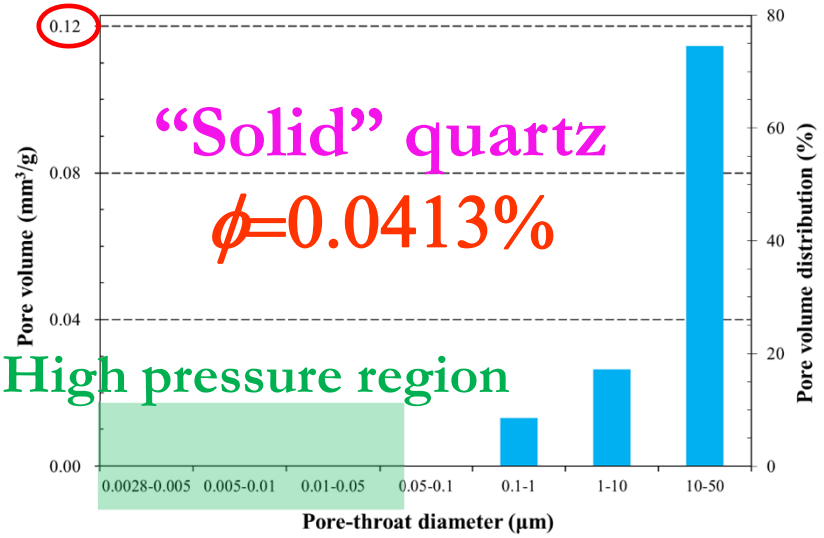

	Expected	Measured. (N=3)
Median pore dia. (nm)	6.8± 0.5	7.13±0.06
Total pore vol. (mL/g)	0.53±0.02	0.576±0.010

Silica alumina

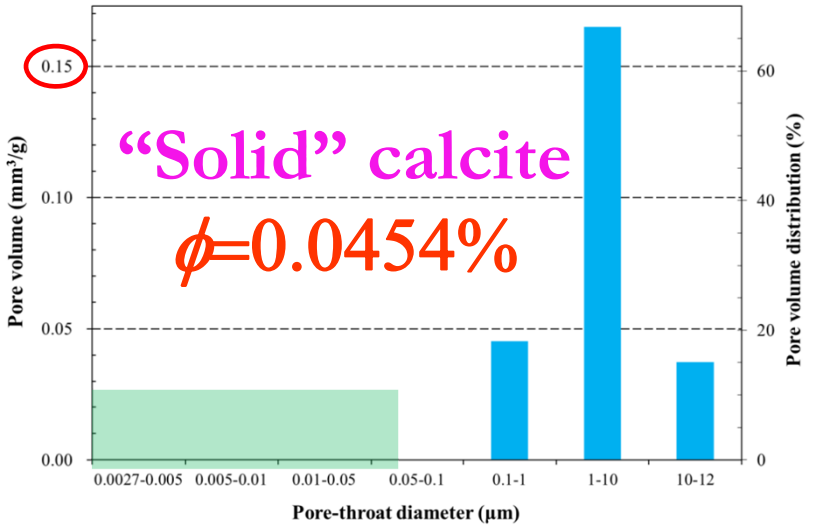

MIP Analysis: PSD vs. Grain Sizes

UNIVERSITY OF TEXAS-ARLINGTON

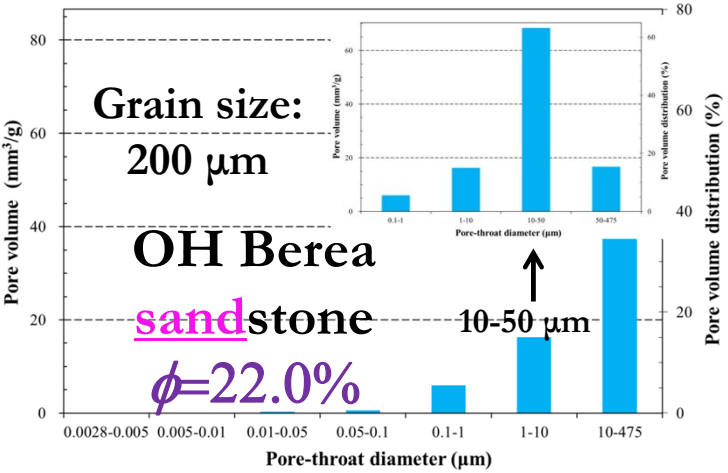

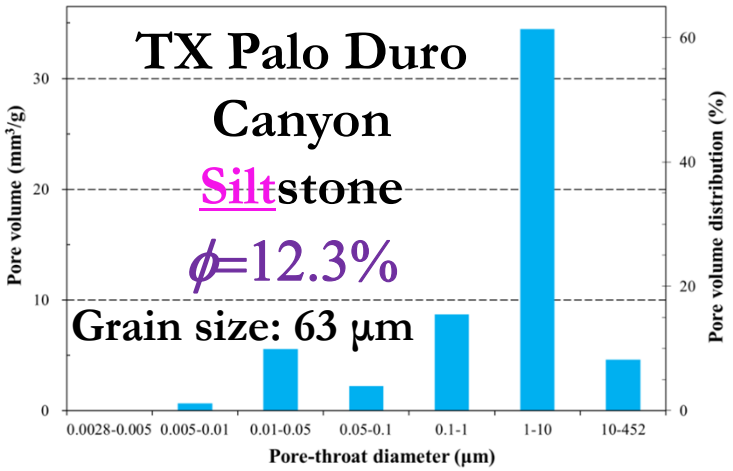

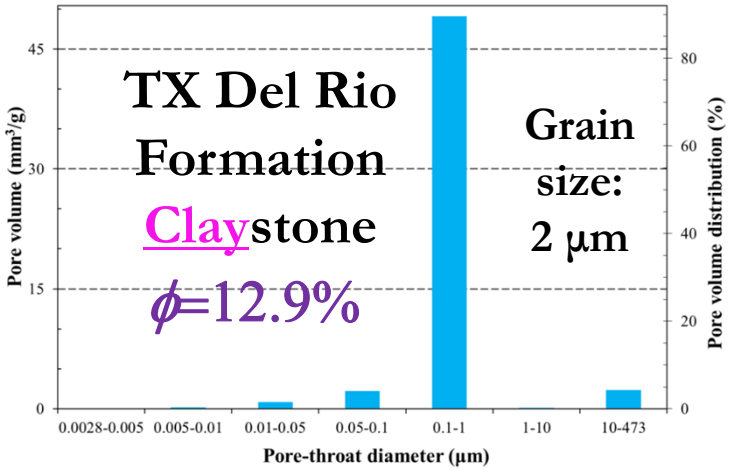

cubic

$d=0.414D$

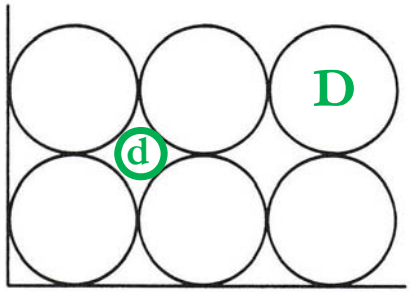

rhombohedral

$d = 0.155D$

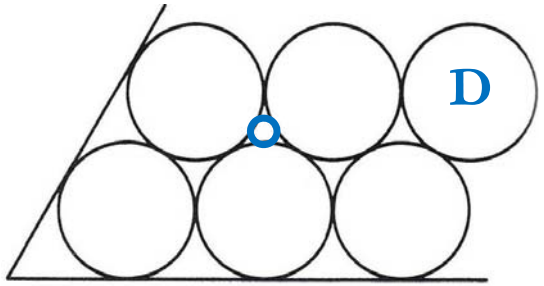

Packing / D	200 μm	63 μm	2 μm	0.1 μm
Cubic / *d*	83	26	0.828	0.041
Rhombohedral / *d*	31	9.7	0.309	0.015

Global Benchmarking Tests: KG²B Project (2015-2017)

UNIVERSITY OF TEXAS–ARLINGTON

Gases vs. liquids
Steady-state vs. transient
Confining pressure

30 labs from 8 countries

1 hr – 5 d

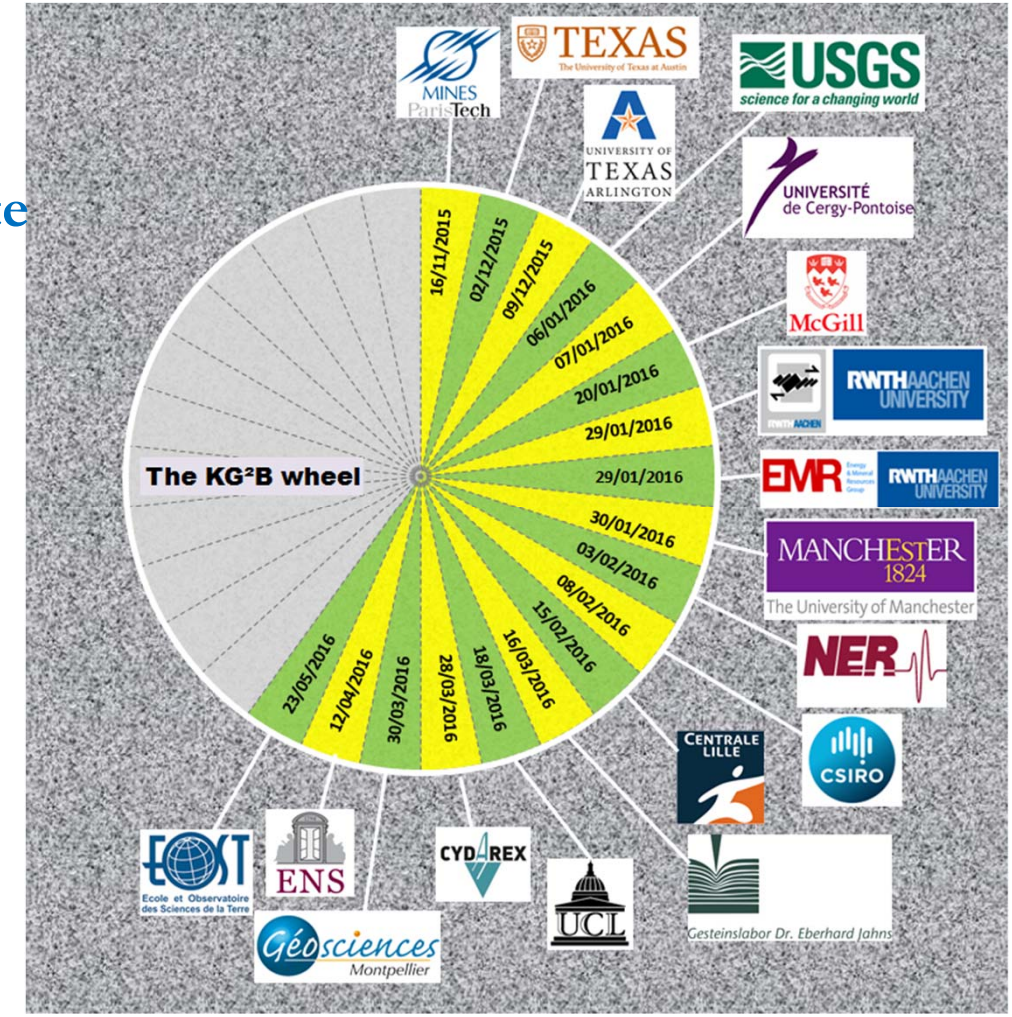

Porosity: 0.80±0.42% (N=31)
Permeability: 1.11±0.57 µD (N=35)

MIP

Porosity: 0.59%
Permeability: 1.08 µD

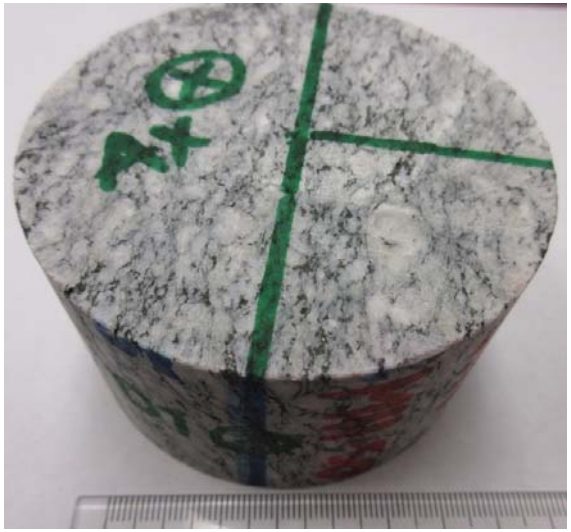

K for Grimsel Granodiorite Benchmark

David et al., GJI, 2018a, b

MIP Results: μm-nm Pore-throat Spectrum for Different Rocks

UNIVERSITY OF TEXAS-ARLINGTON

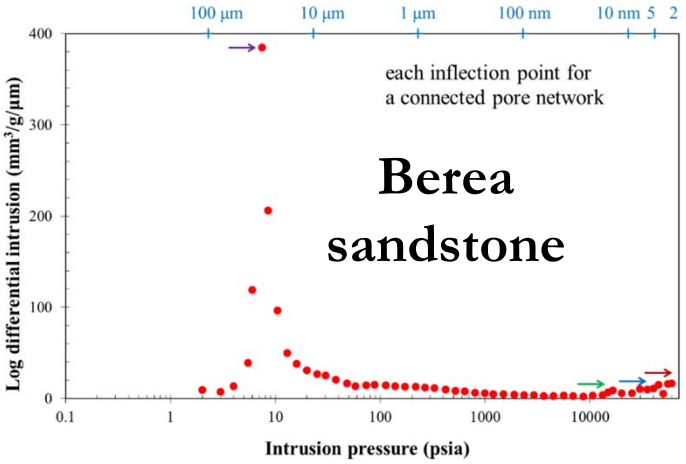

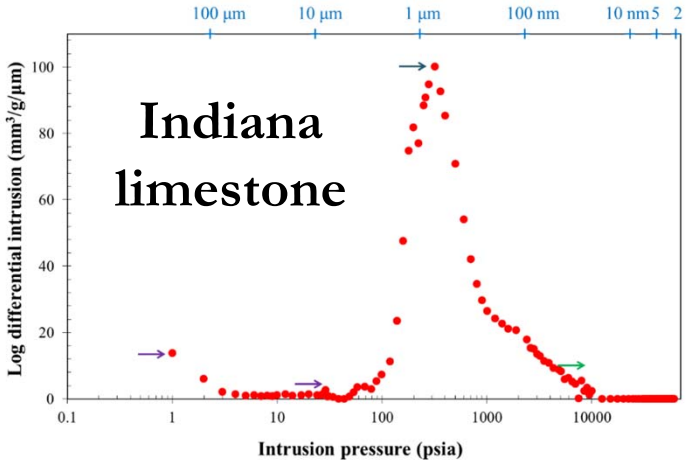

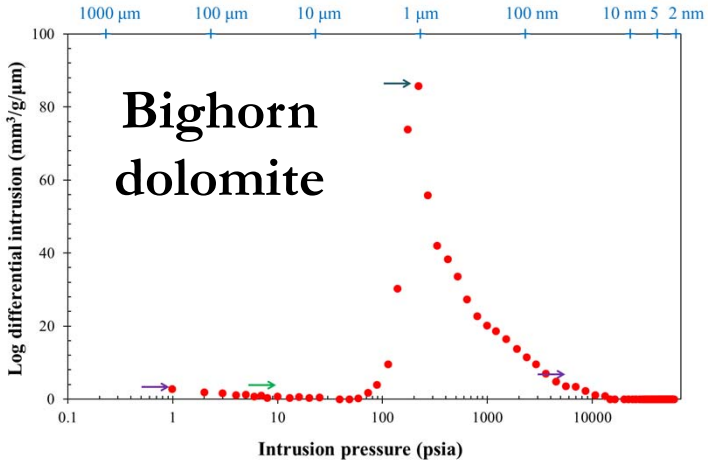

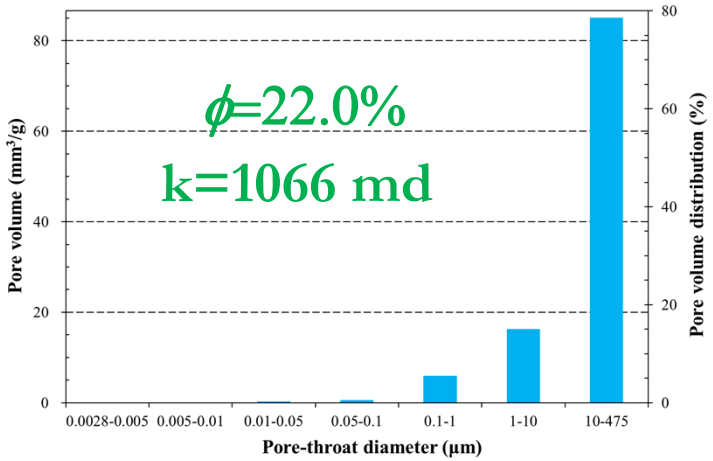

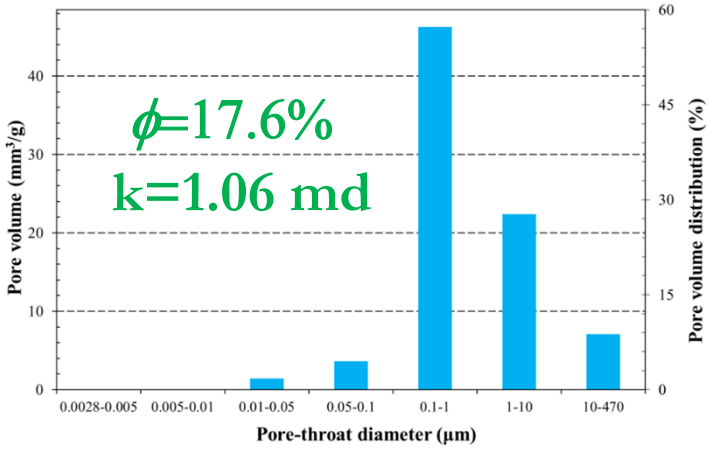

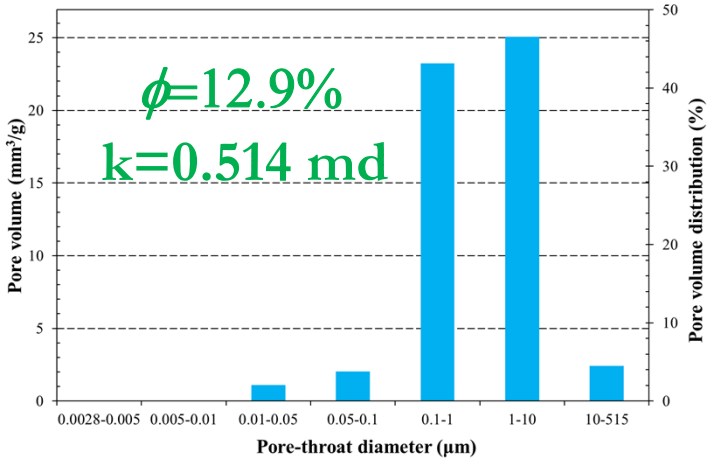

Eagle Ford Stratigraphy: Pore-throat Size Distribution

UNIVERSITY OF TEXAS-ARLINGTON

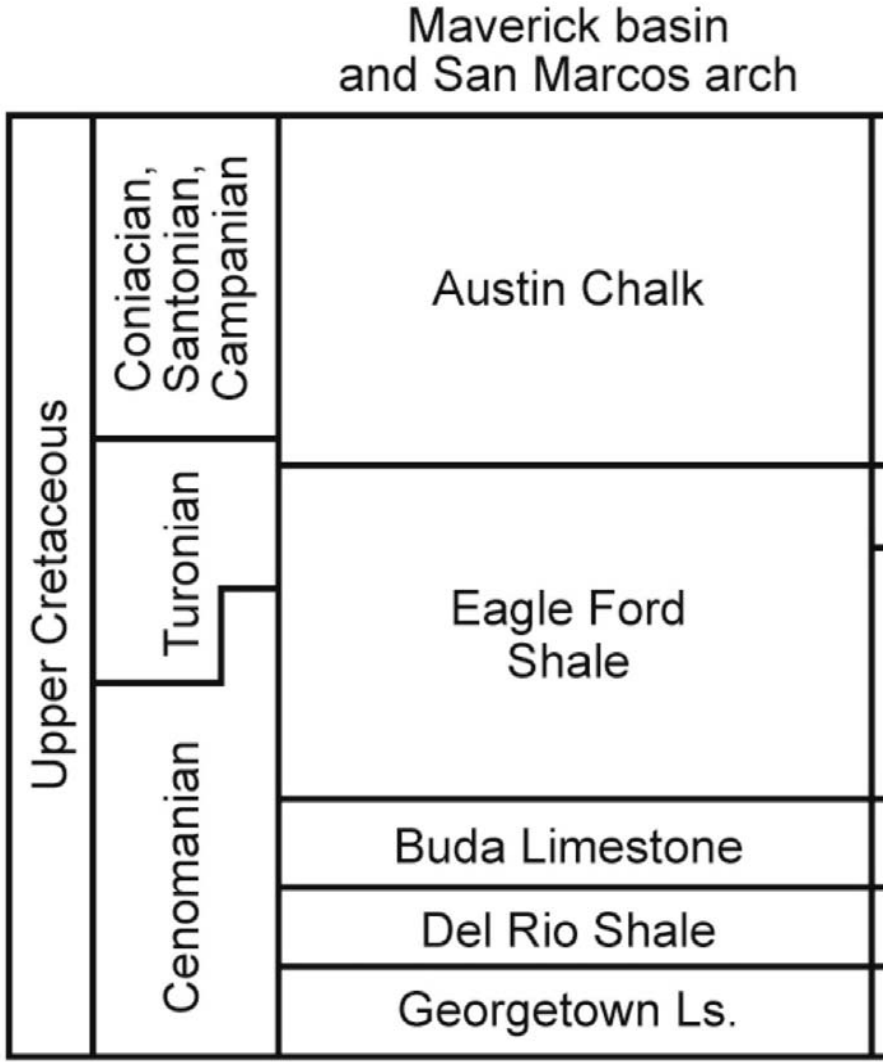

Organic matter-related

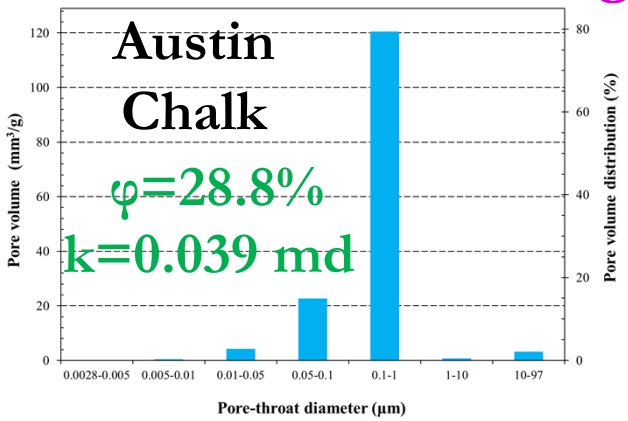

100-1000 nm

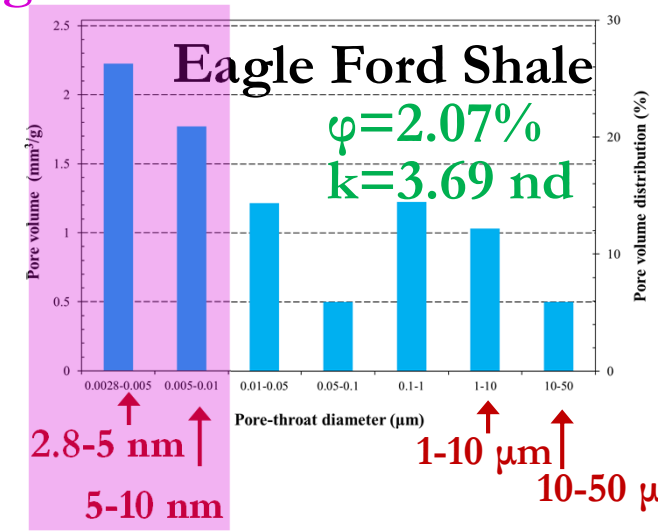

100-1000 nm

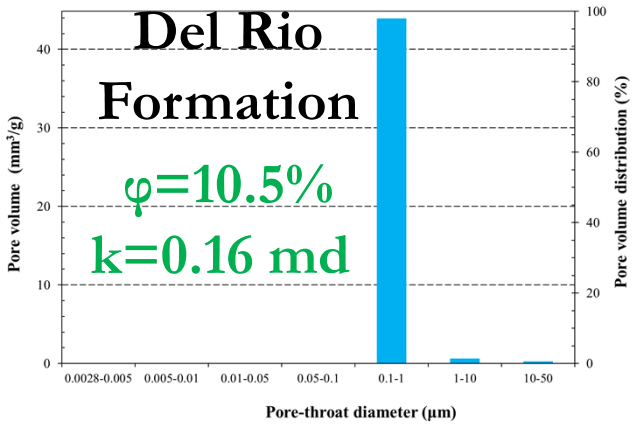

10-50 nm

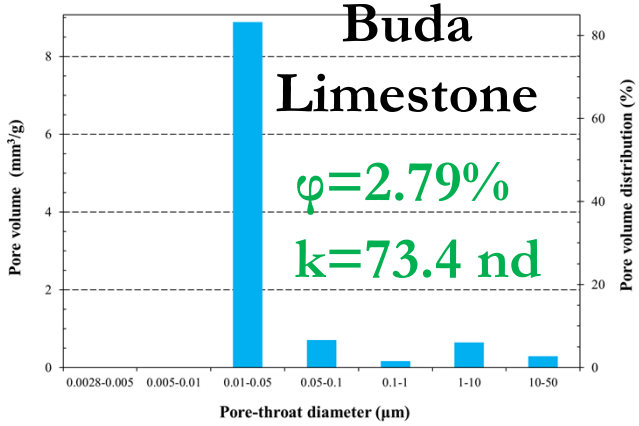

Barnett Formation: Pore-throat Size Distribution

UNIVERSITY OF TEXAS-ARLINGTON

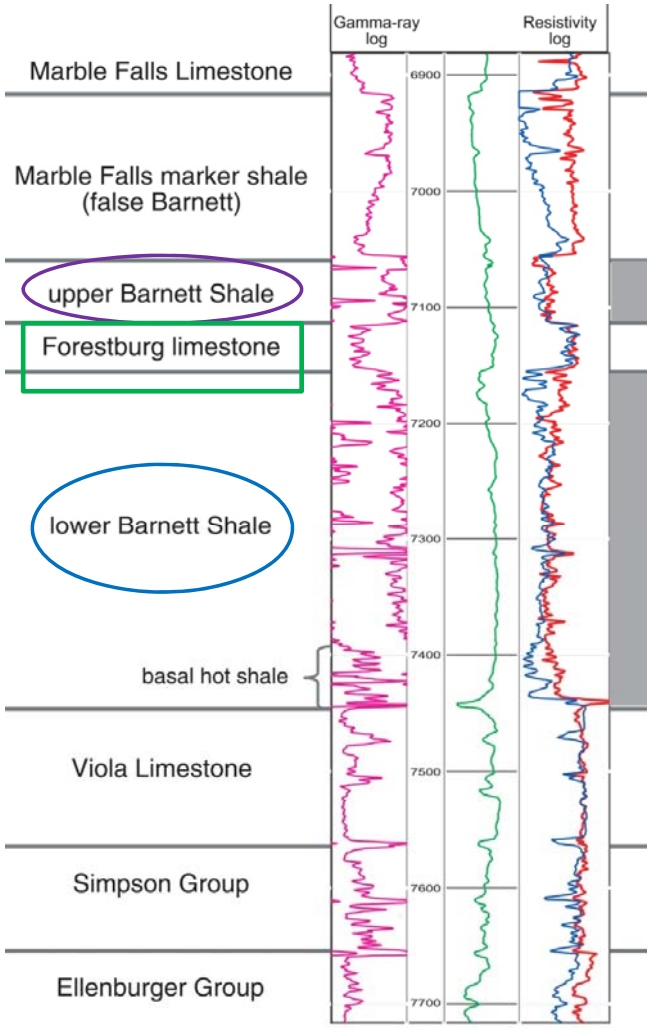

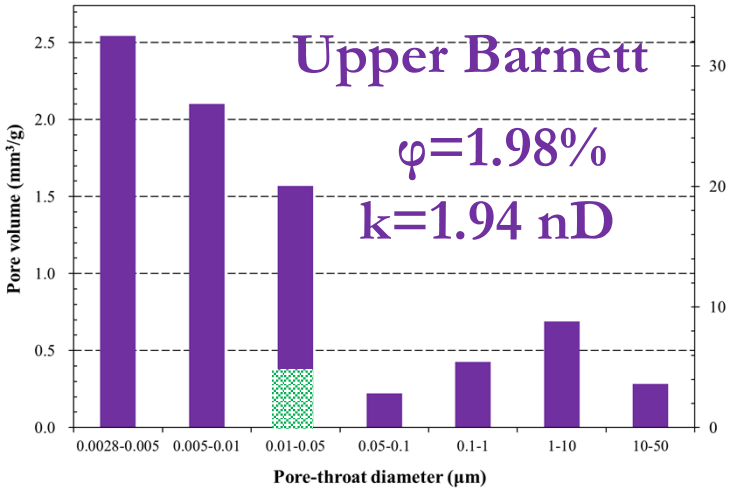

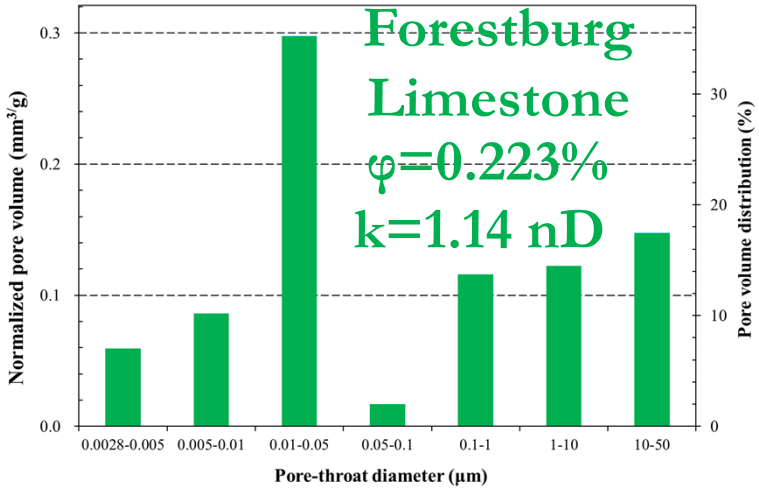

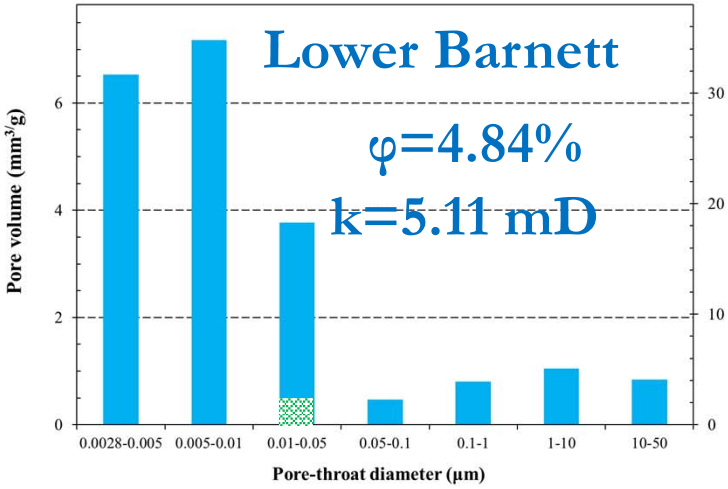

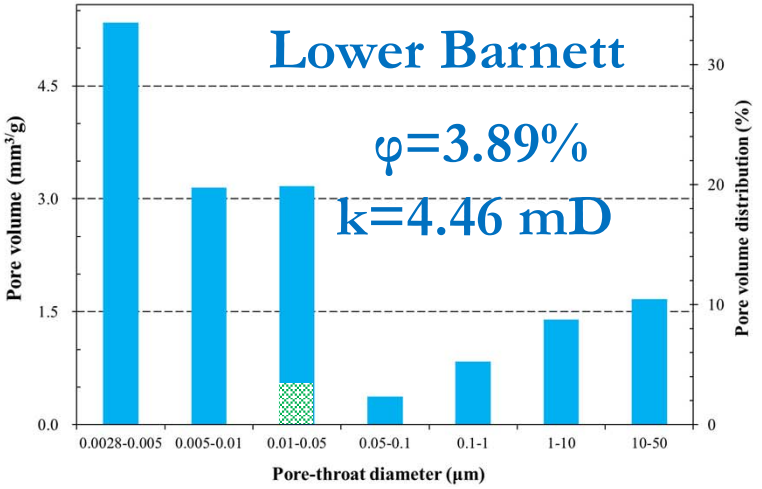

MIP Analysis: Shale Pore Structure and Network

UNIVERSITY OF TEXAS-ARLINGTON

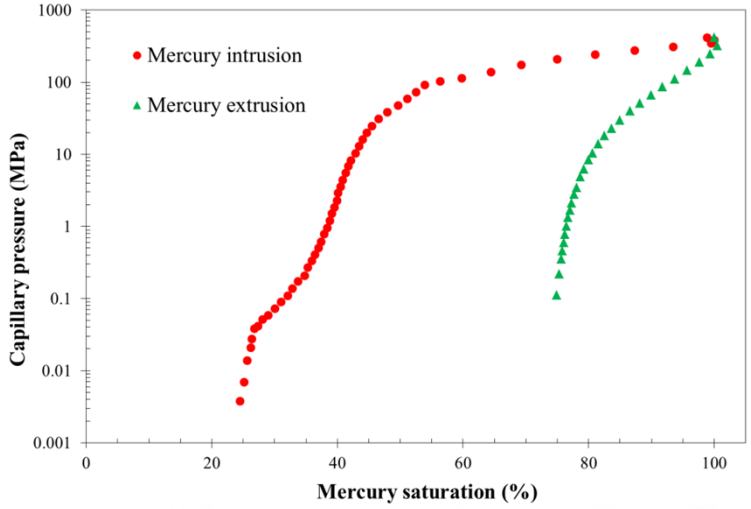

Barnett Shale
Blakely #1 7219

ϕ=5.09%

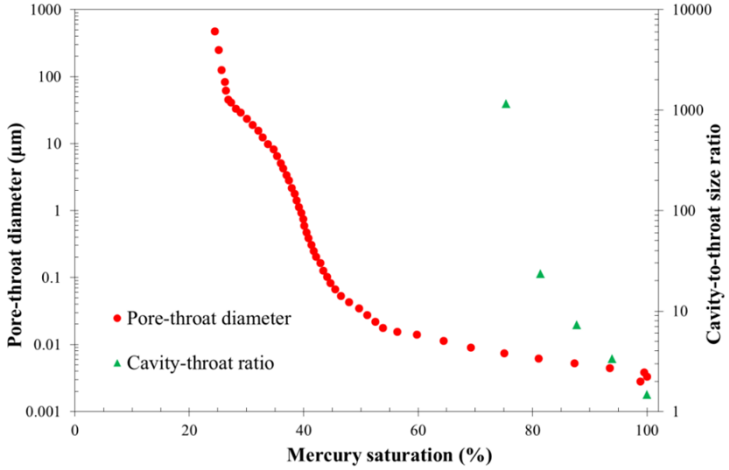

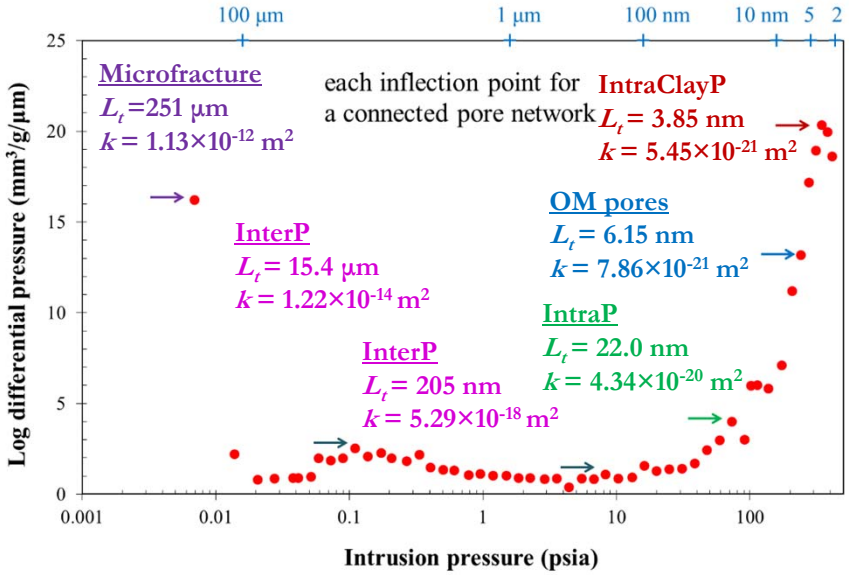

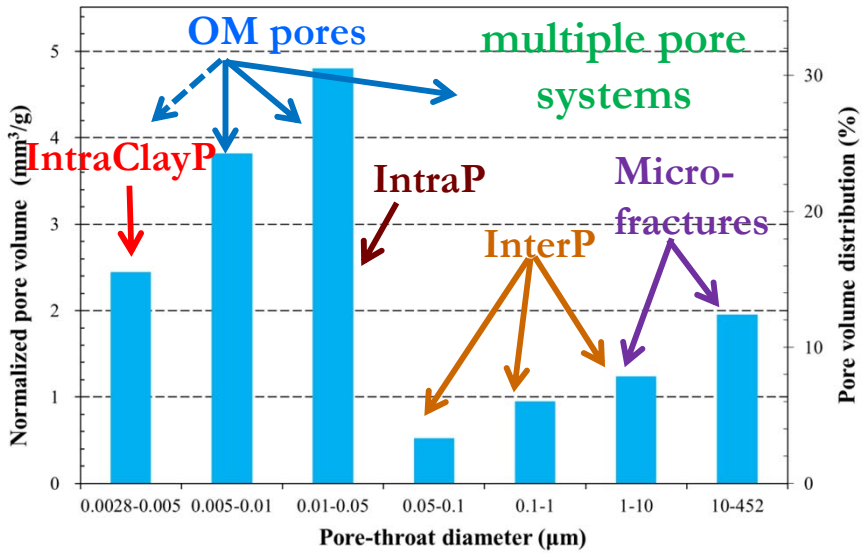

Imbibition Test: The Square-Root-of-Time relationship

UNIVERSITY OF TEXAS-ARLINGTON

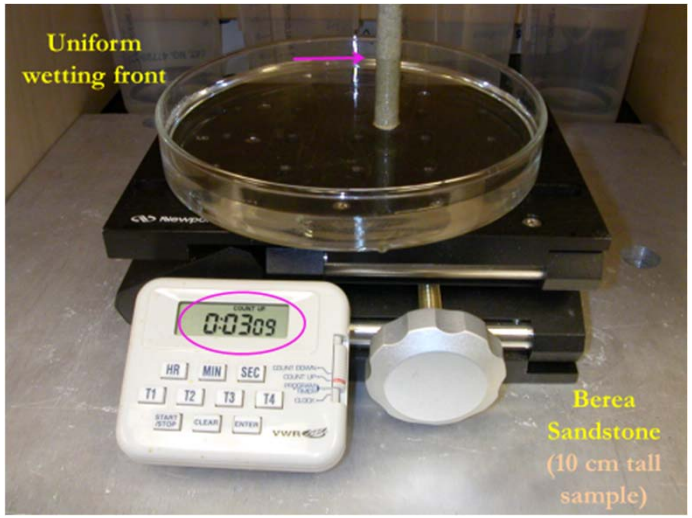

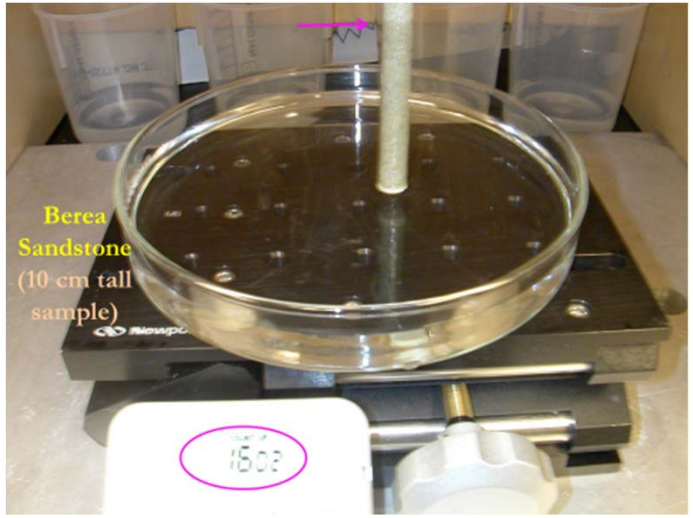

Berea sandstone

"homogeneous"

well-connected pore space

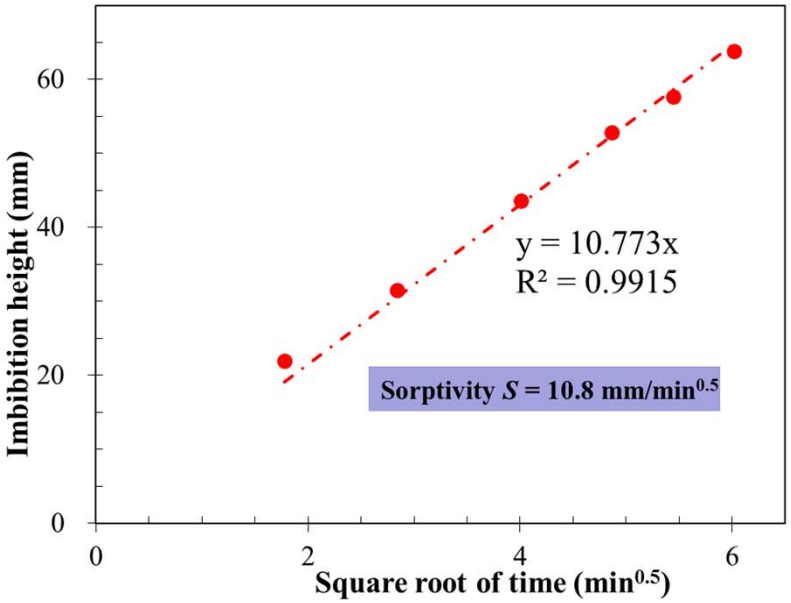

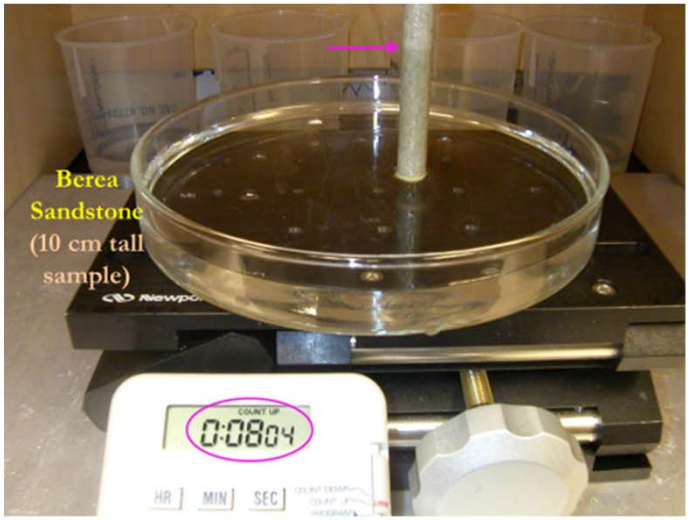

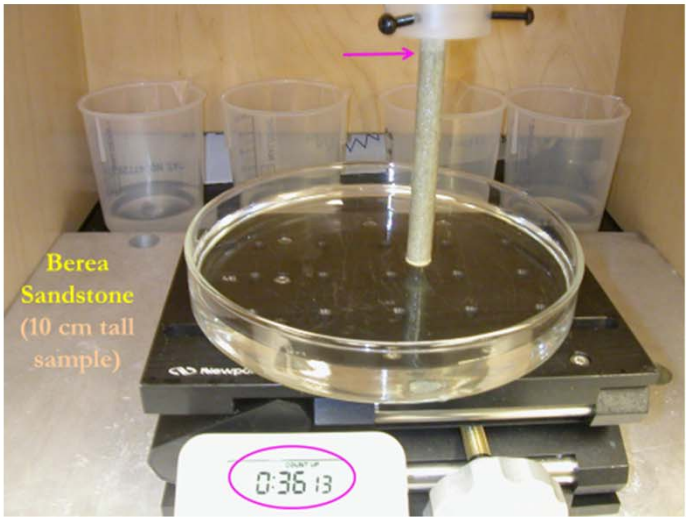

Imbibition Test to Probe Pore Connectivity

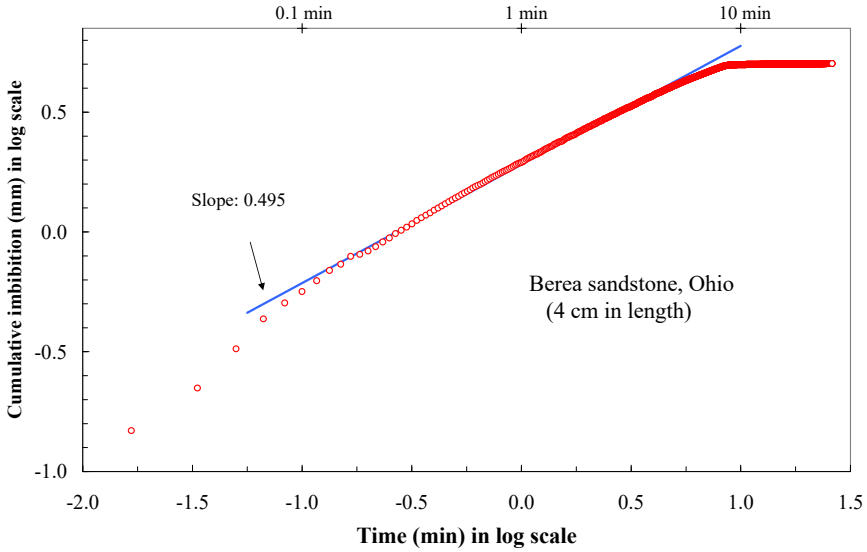

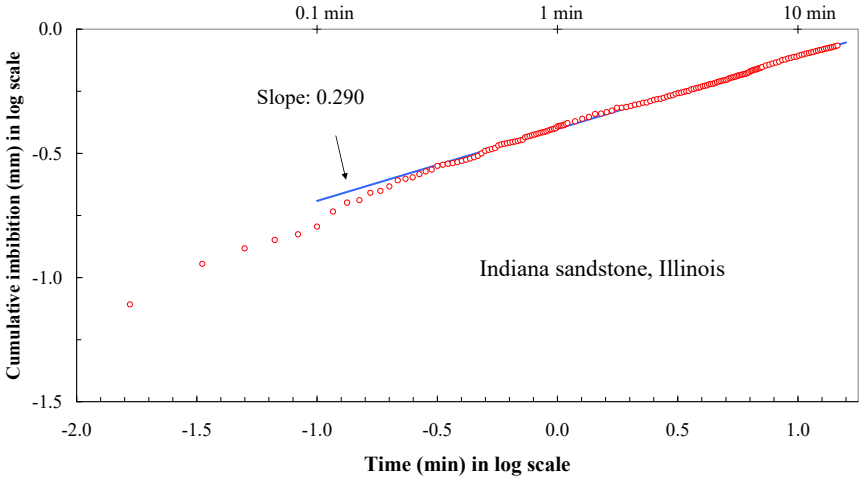

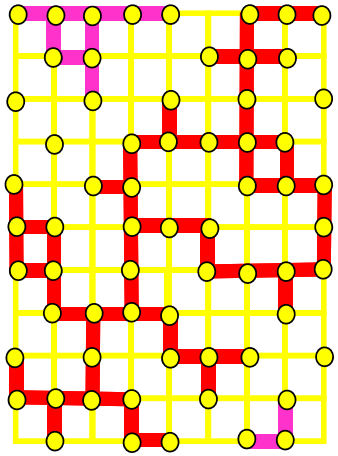

p = 0.66

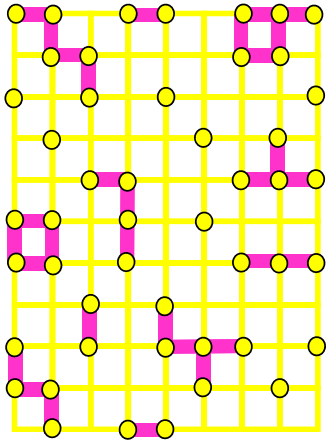

p = 0.5

Percolation theory: the study of how pore connections affect the resultant macroscopic properties

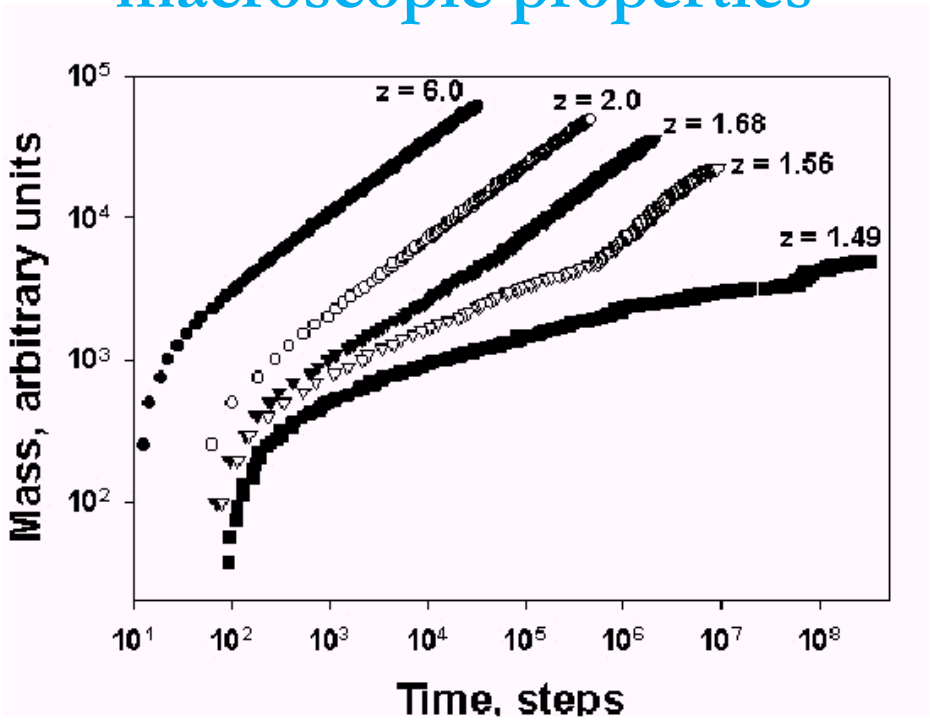

Mixed Wettability and Associated Pore Structure

UNIVERSITY OF TEXAS–ARLINGTON

- Dalmatian wettability behavior
- Variable at um scale
- Complex interplay of wettability and pore size

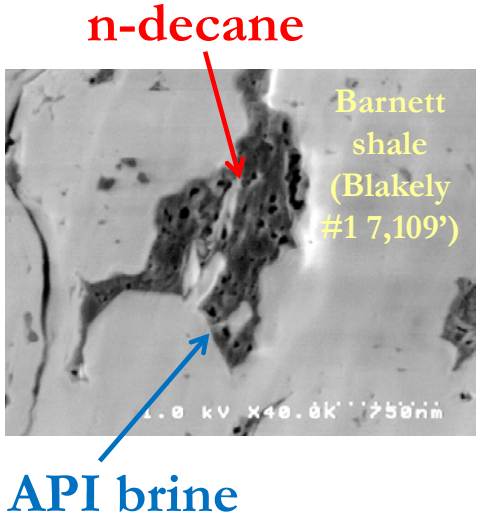

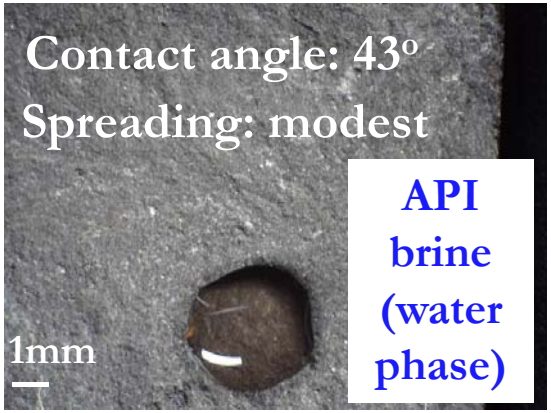

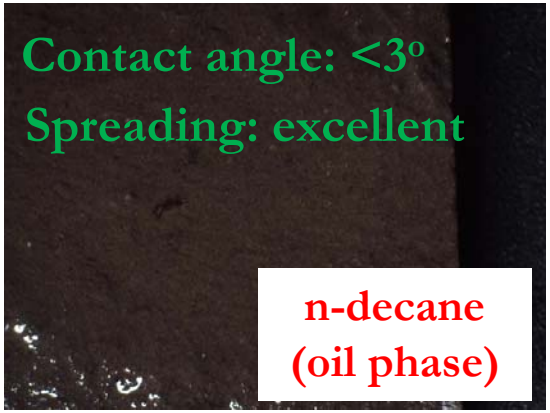

Fluid spreading behavior in a typical mudrock

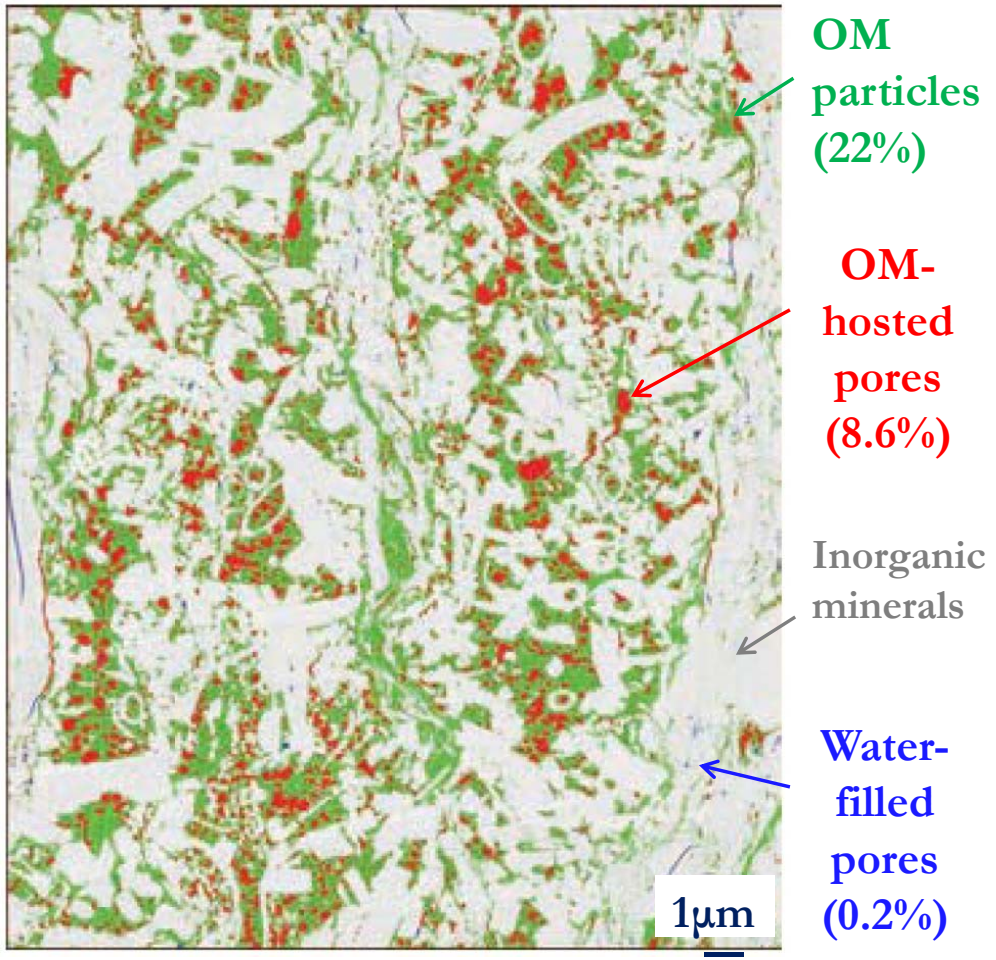

Wolfcamp: SEM (Wall et al., 2016)

Pore Connectivity: Imbibition

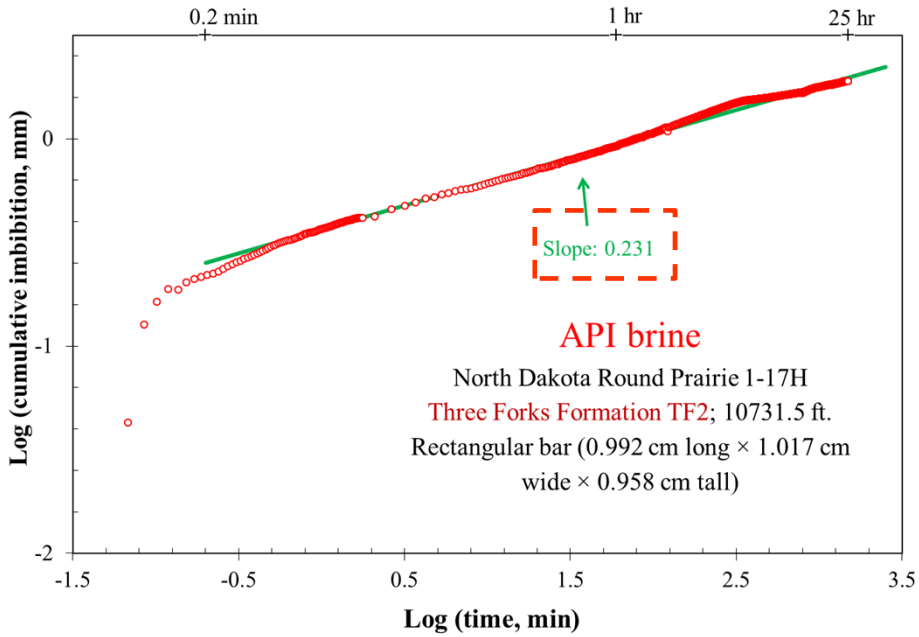

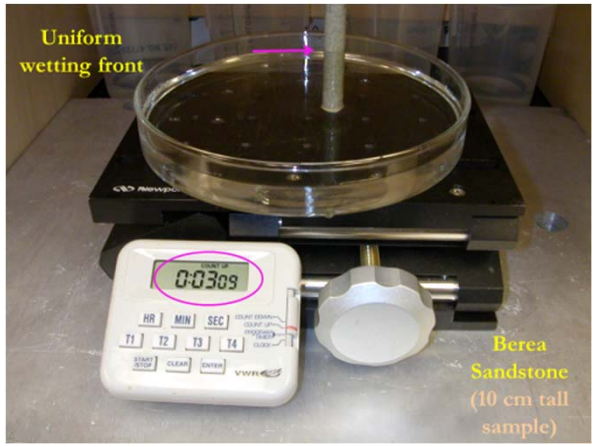

Hu et al., JH, 2002

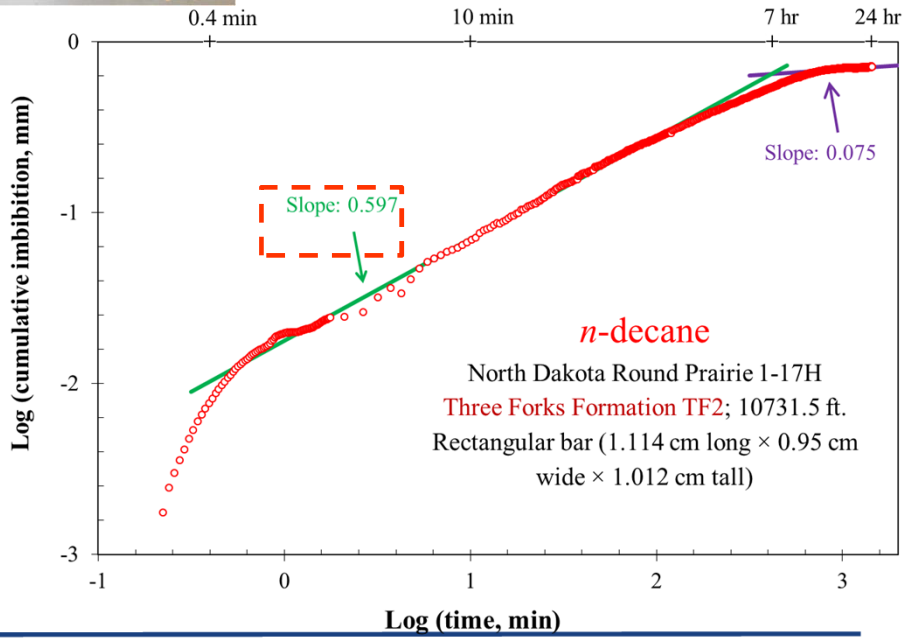

- ✓ More "oil-wet"
- ✓ Low pore connectivity for brine (slope ~1/4)
- ✓ High pore connectivity for n-decane (slope ~1/2; but only travel for 1 cm after 7 hrs)

Wettability-based Fluids and Tracers

UNIVERSITY OF TEXAS-ARLINGTON

- **API brine (8 wt% NaCl+2 wt% $CaCl_2$) [w*ater-wet*]**
  - ✓ ReO_4^- (0.553 nm)
  - ✓ Anionic Sb-complex (0.89 nm)
  - ✓ Cationic Ru-complex (1.0 nm)
  - ✓ CdS nanoparticles (5–10 nm)

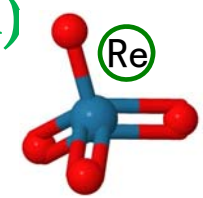

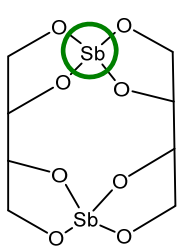

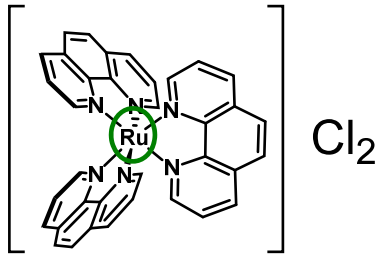

$C_{36}H_{24}N_6Ru_1Cl_2$

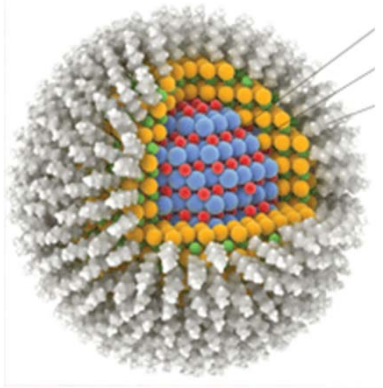

CdS (5–10 nm)

- **n-decane: toluene [*oil-wet*]**
  - ✓ Organic-I
  - ✓ Organic-Re
  - ✓ CeF_3 nanoparticles (10–12 nm)

0.23 nm

1.393 nm × 0.287 nm × 0.178 nm

$CH_3(CH_2)_8CH_2I$

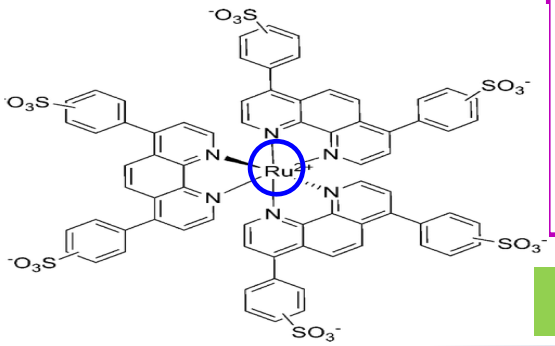

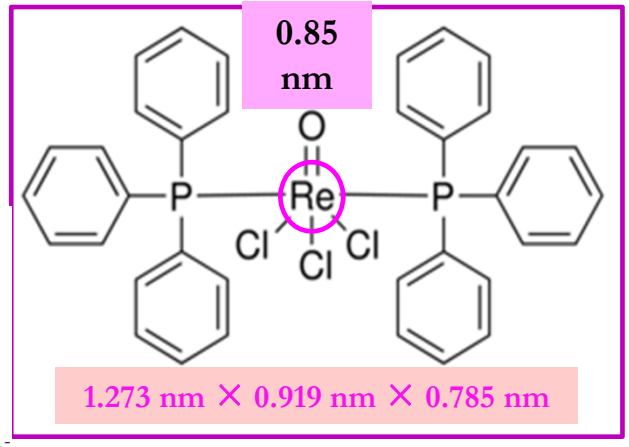

1.273 nm × 0.919 nm × 0.785 nm

- **Tetrahydrofuran–zewittering**
  - ✓ Ru-complex (2.42 nm)

Hu et al., J. Nano. Nanotech., 2017

Different Tracer Tests for Process-Level Understanding

UNIVERSITY OF TEXAS-ARLINGTON

Imbibition

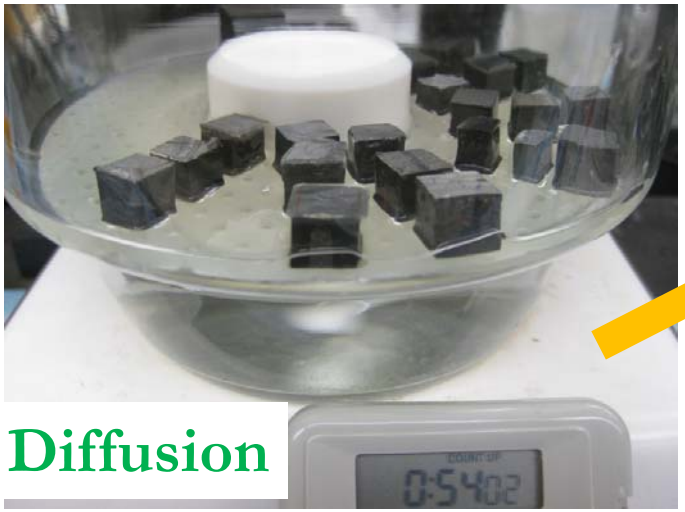

Diffusion

Laser Ablation-Inductively Coupled Plasma-Mass Spectrometry (LA-ICP-MS)

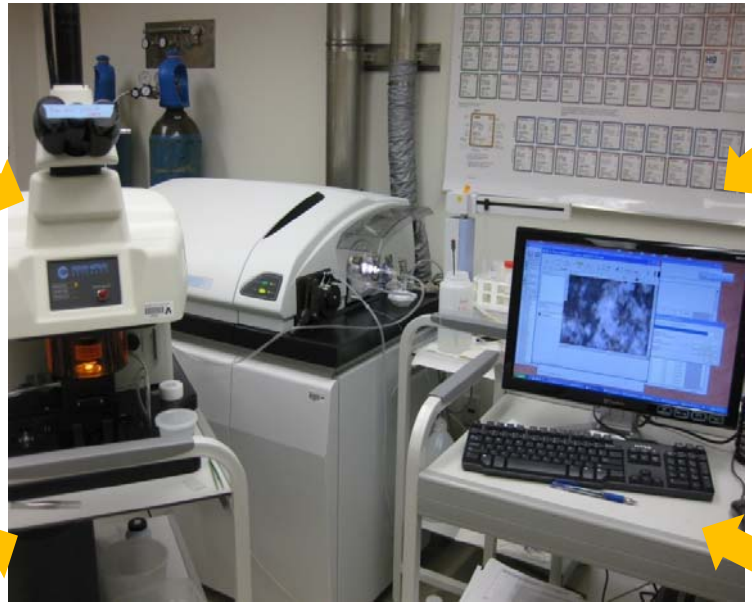

Hu et al., VZJ, 2004; GJ, 2012

Vacuum saturation

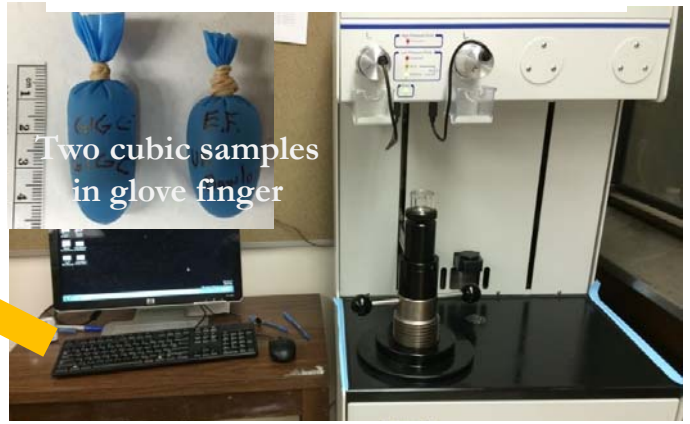

High-pressure impregnation

Liquid Tracer Diffusion Tests

UNIVERSITY OF TEXAS-ARLINGTON

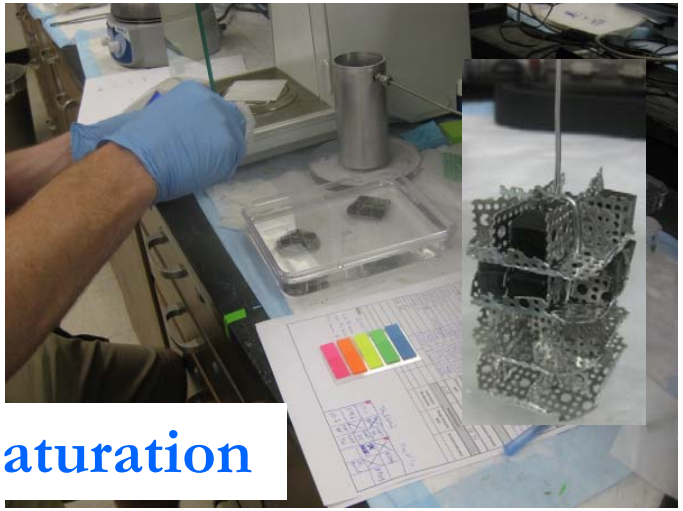

Vacuum saturation

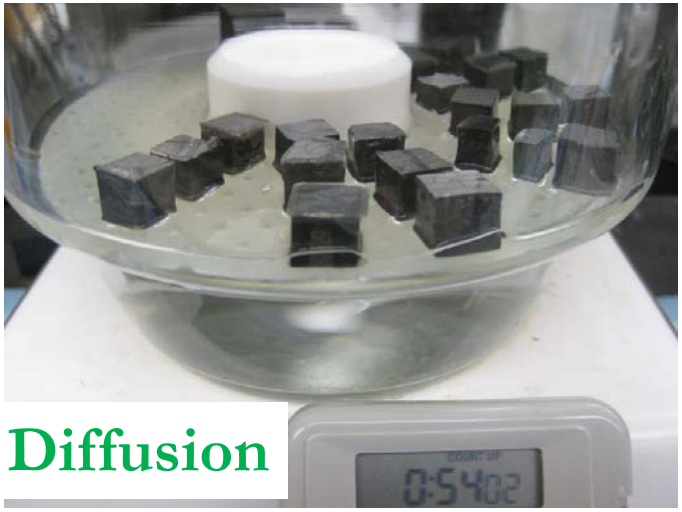

Diffusion

freeze drying

Laser Ablation-Inductively Coupled Plasma-Mass Spectrometry (LA-ICP-MS)

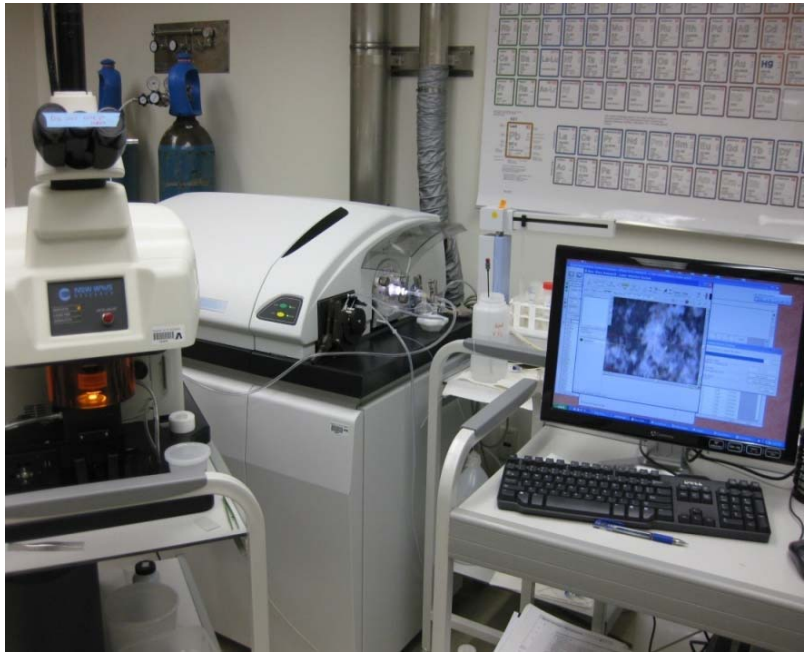

Hu et al., VZJ, 2002; GJ, 2012

Liquid Tracer Diffusion in Saturated Mudrock

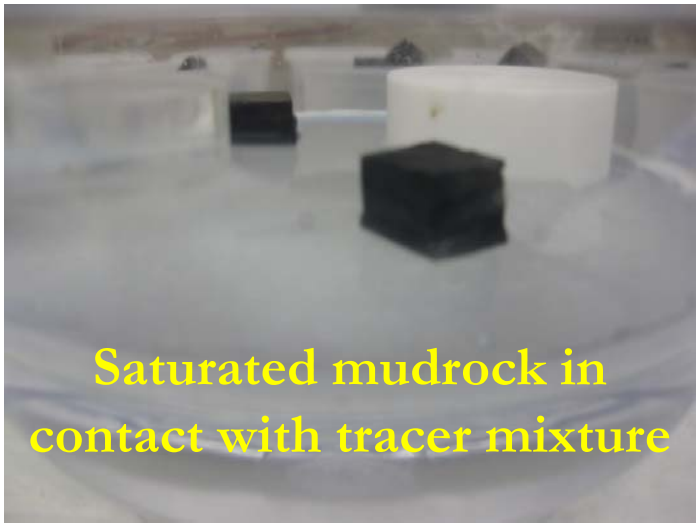

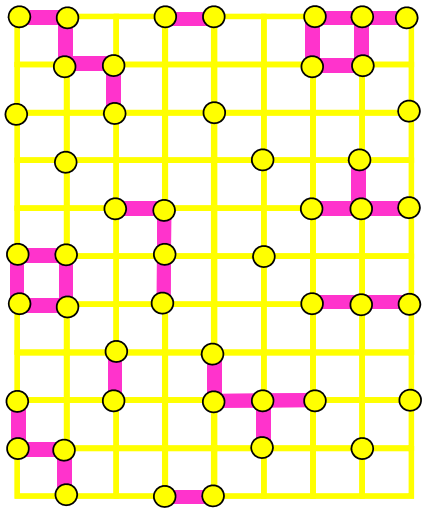

$$\tau = \frac{D_0}{De}$$

$$\frac{C}{C_0} = \frac{1}{2} erfc \frac{x}{2\sqrt{D_e t}}$$

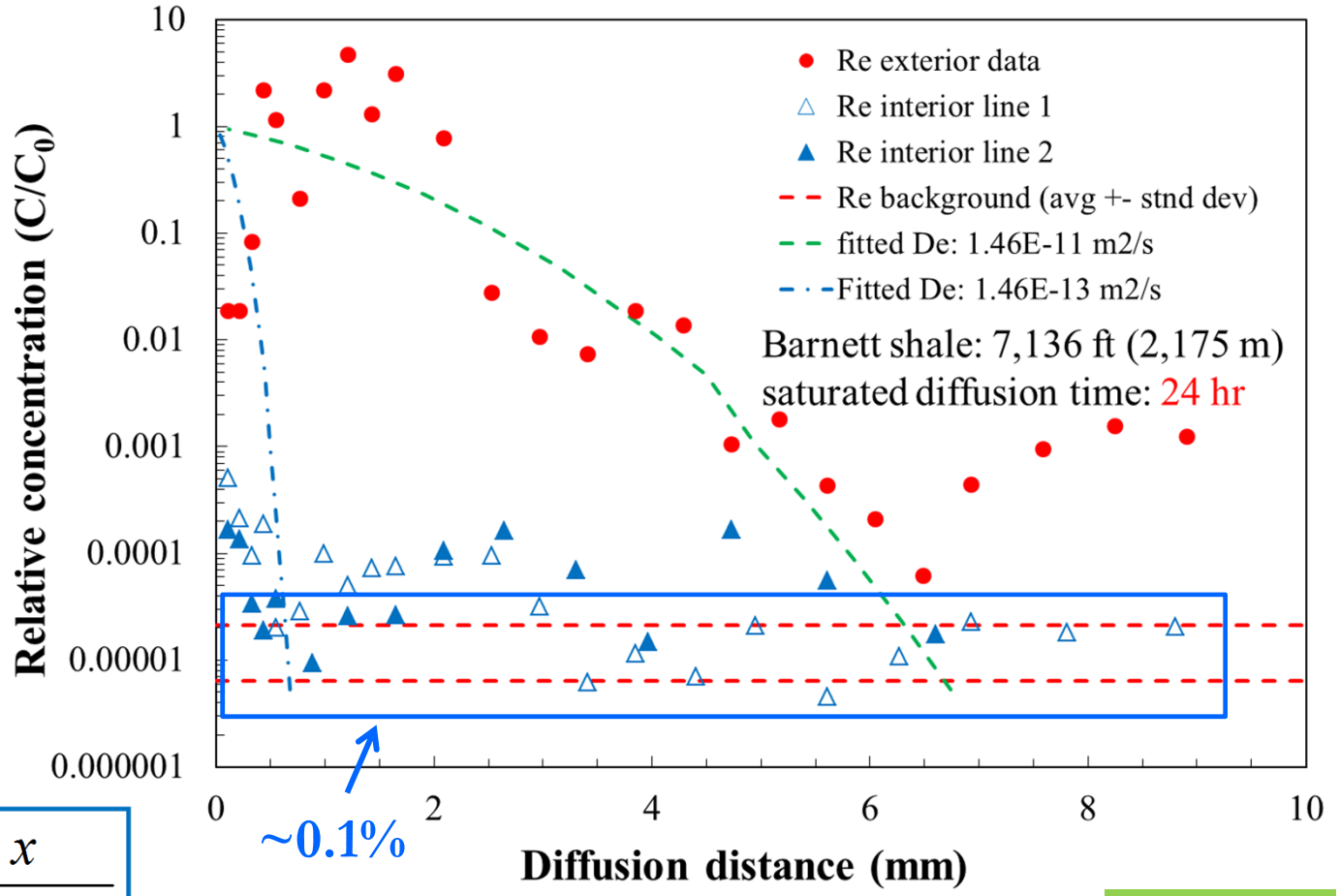

τ: 1.13 (exterior); 35.6 (interior)

Hu et al., JGR, 2015

Laser Ablation-ICP-MS Tracer Mapping

UNIVERSITY OF TEXAS-ARLINGTON

10 mm-sided cube

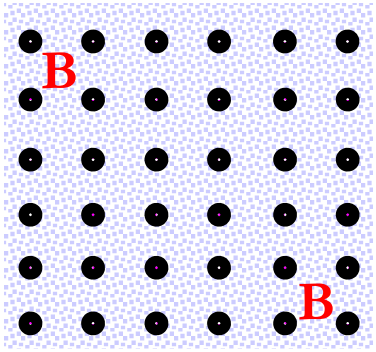

Bottom (tracer-contacted) face conc. Check

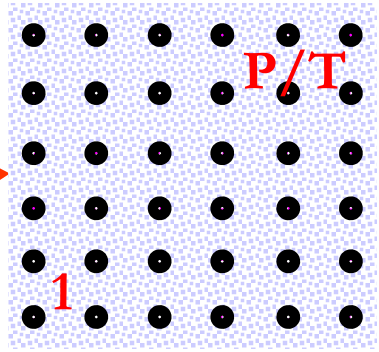

Conc. check of top face (either Parallel or Transverse to lamination)

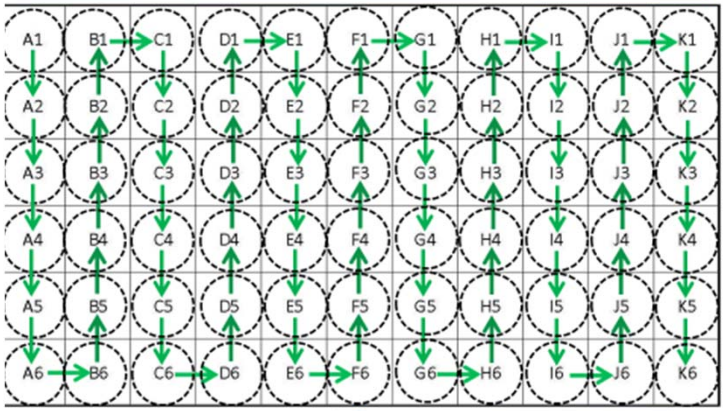

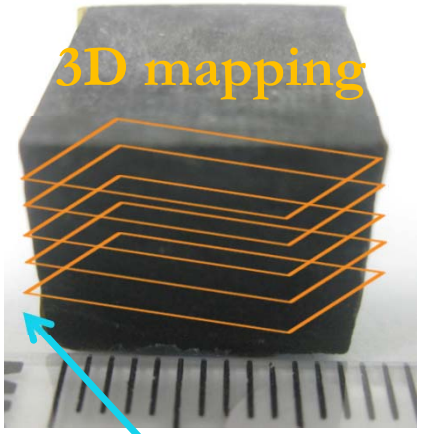

Interior face(2D mapping)

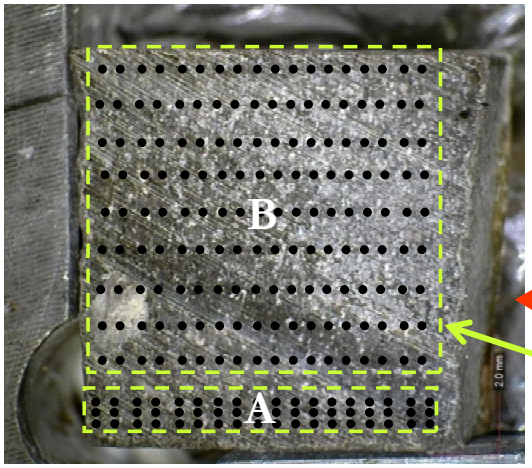

Remove epoxy on the wall to map side face

Cut the sample dry to expose the interior face

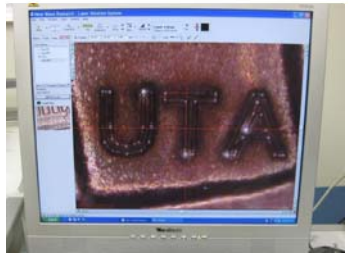

Tracer mapping grids

Hu et al., 2015; 2018; 2019

Non-wetting Fluid: Effective Porosity Effect

UNIVERSITY OF TEXAS-ARLINGTON

Re background: 1.29±1.24 mg/kg

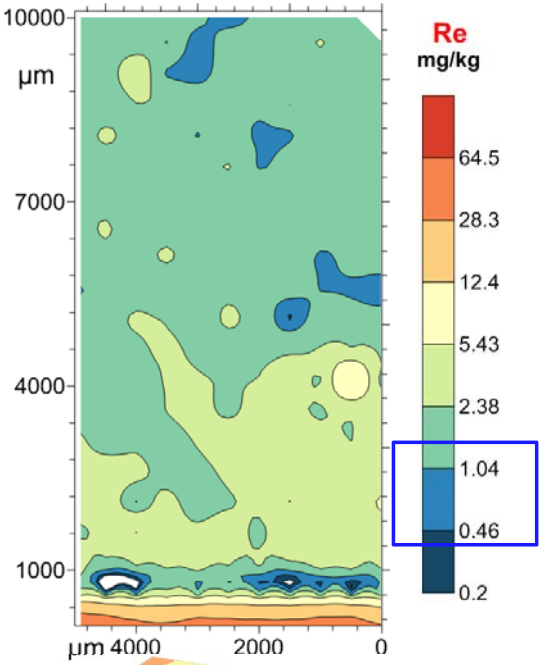

Cs background: 8.85±4.20 mg/kg

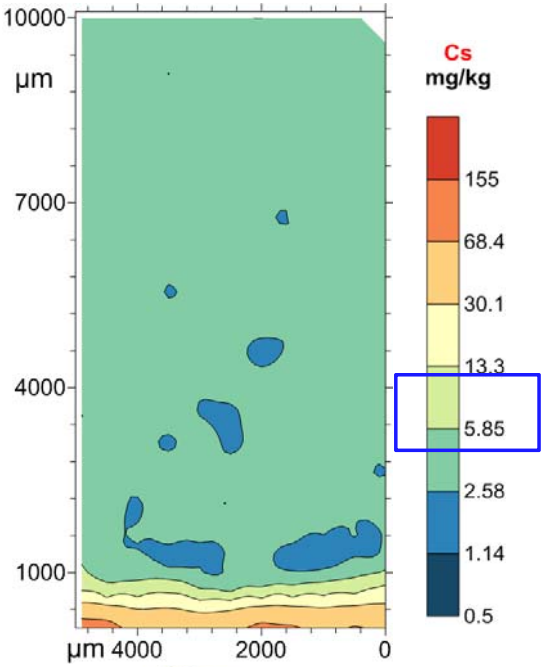

Ce background: 51.0±33.6 mg/kg

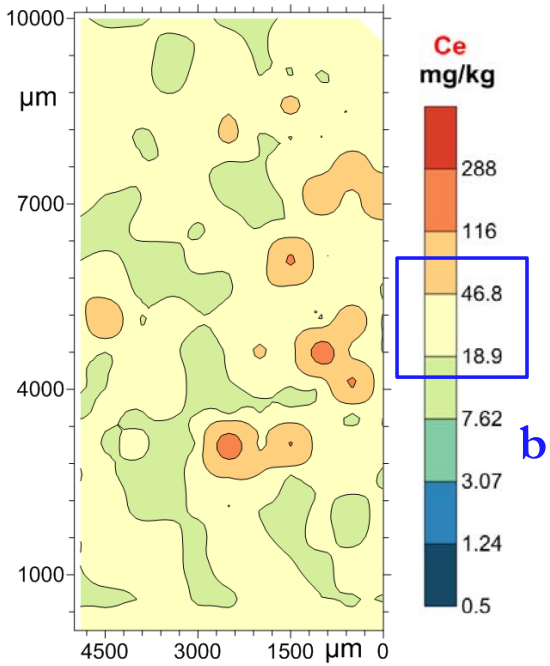

background levels

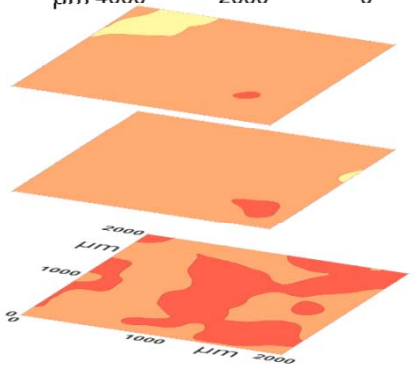

5–71 μm

1–5 μm

0–1 μm

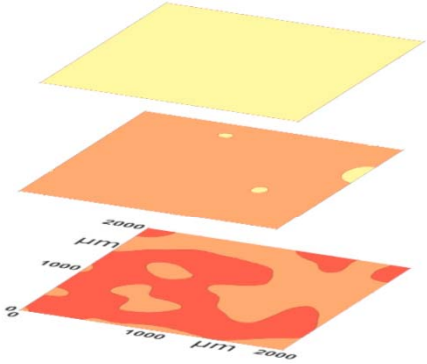

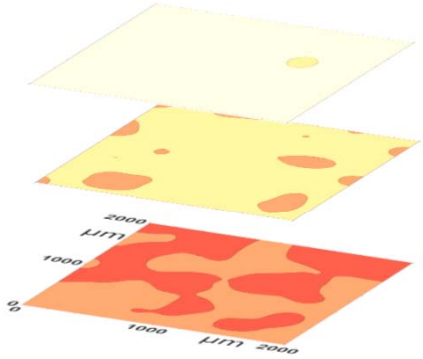

Barnett Blakely#1 7109' brine imbibition 94 hrs

Steric Entanglement: Molecular Size Effect

UNIVERSITY OF TEXAS-ARLINGTON

n-decane fluid Niobrara: 17-1A H

vacuum saturation + high pressure intrusion

Pore-throat size distribution

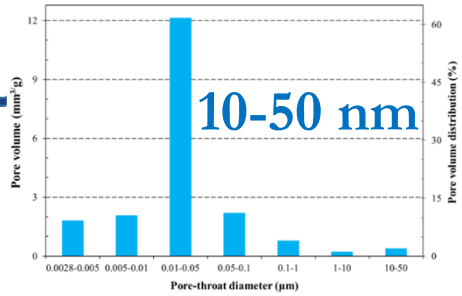

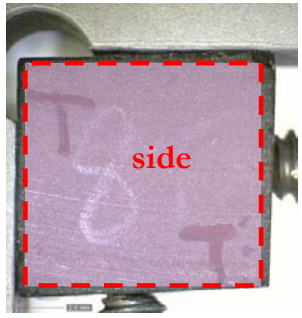

I (mg/kg; sampling point)

bkdg: 0.50±0.52 (9); side: 15.3±4.03(49)

interior: 7.10±3.01 (180) for 44.6±17.0%

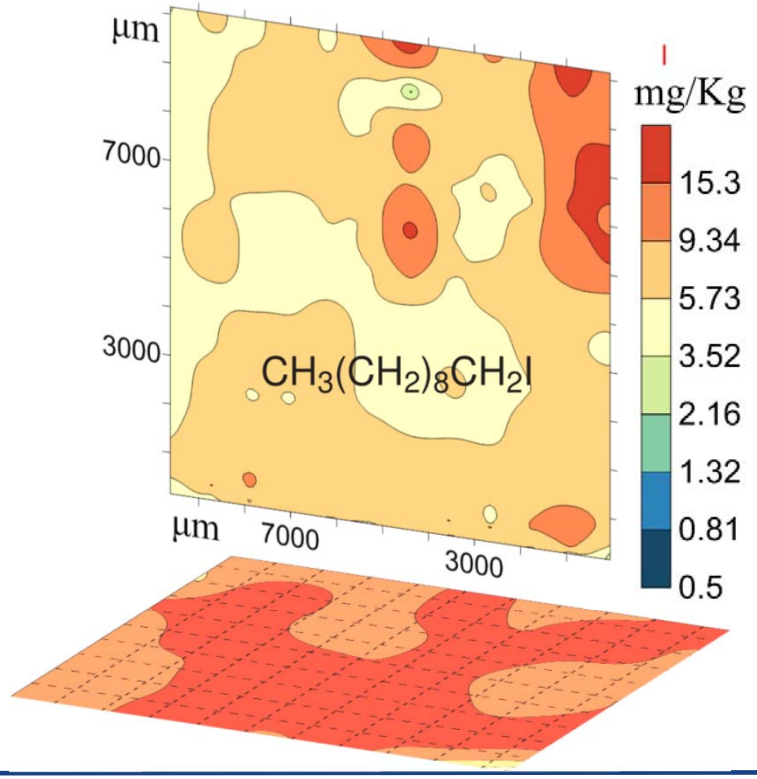

Re (mg/kg; sampling point)

bkdg: 1.55±1.46 (9); side: 675±398(49)

interior: 3.77±5.45 (180) for 0.33±0.58%

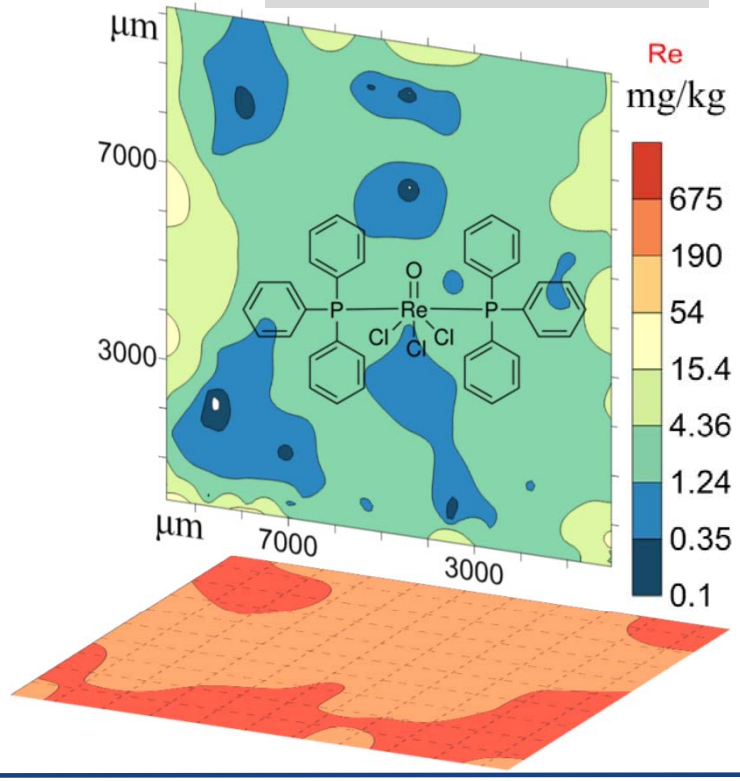

Steric Entanglement: Molecular/Particle Size Effect

UNIVERSITY OF TEXAS–ARLINGTON

Niobrara core 8-2A H (P)

Fluid: API brine

Diffusion time: 25 hrs

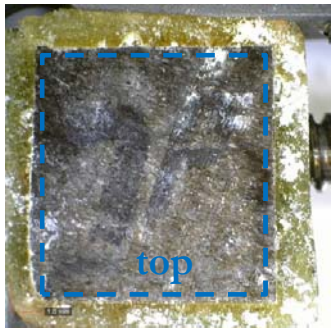

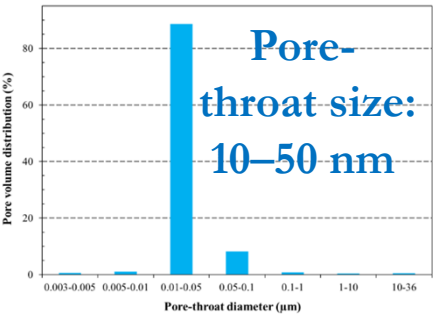

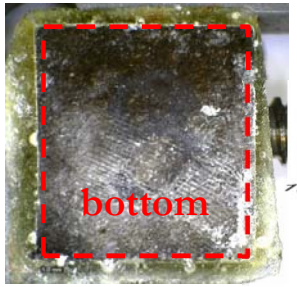

ReO_4^- (0.553 nm)

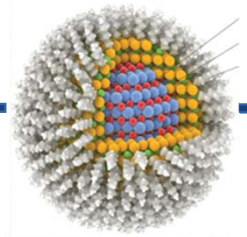

CdS (5–10 nm)

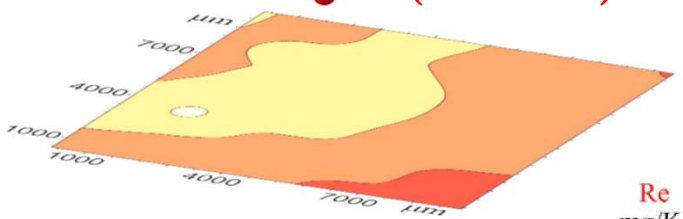

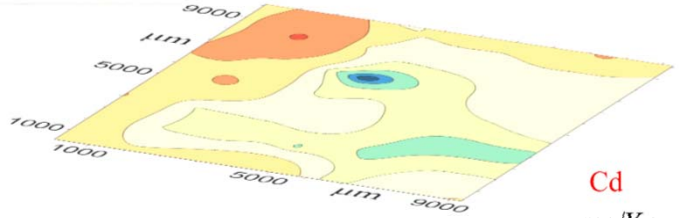

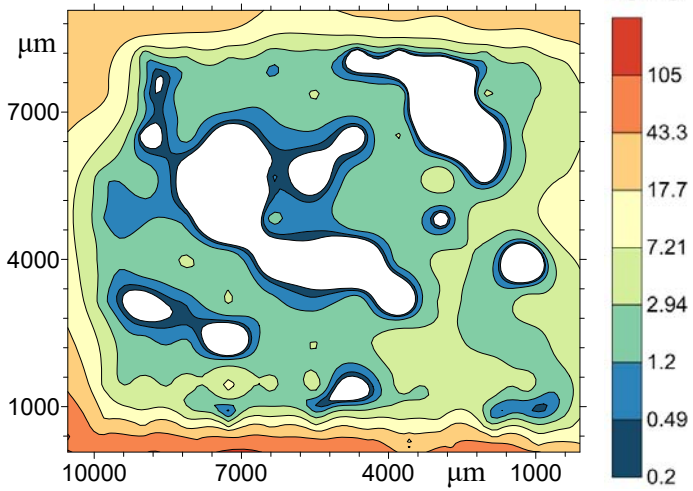

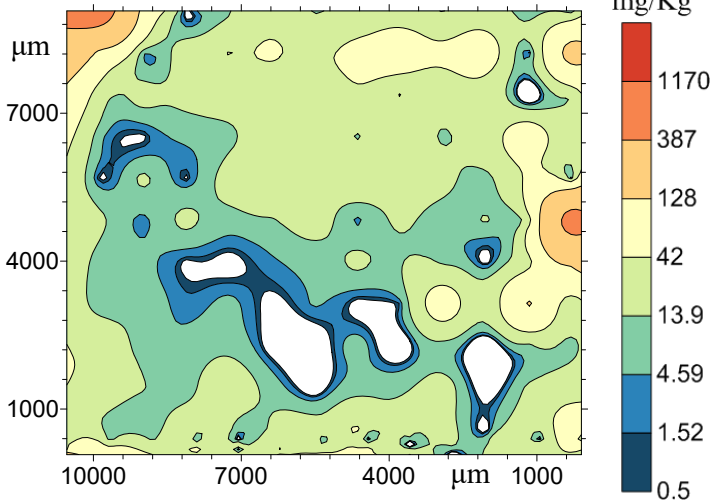

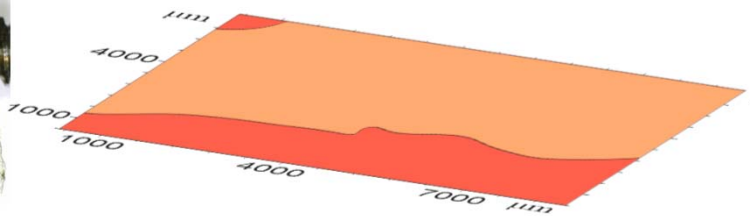

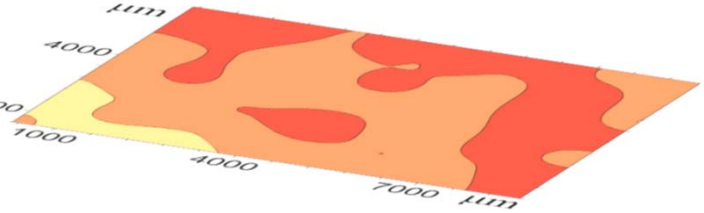

Small Angle Neutron Scattering (SANS): Contrast Matching

UNIVERSITY OF TEXAS-ARLINGTON

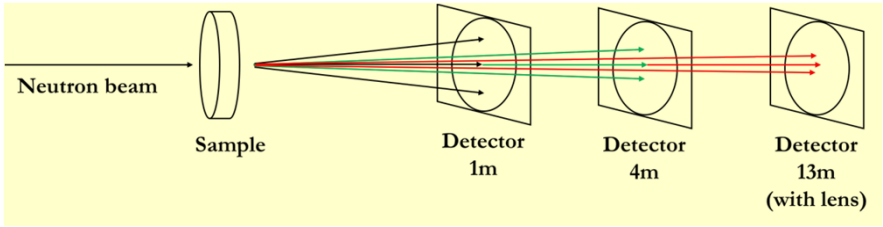

- Detect both connected and closed pores
- Obtain full-scale nm-μm pore diameters
- Quantify hydrophilic vs. hydrophobic pore space
- Investigate reservoir P-T condition

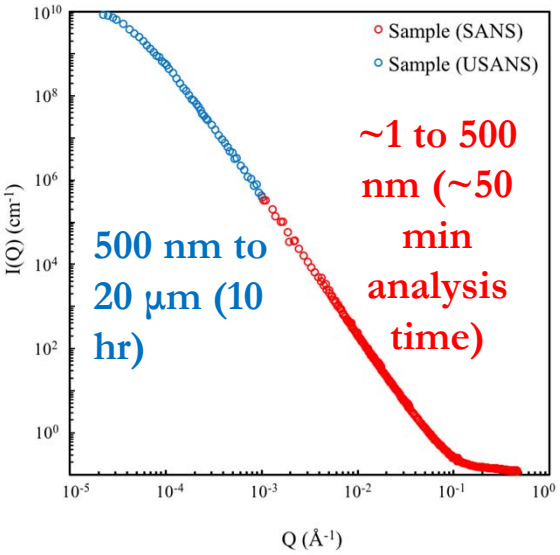

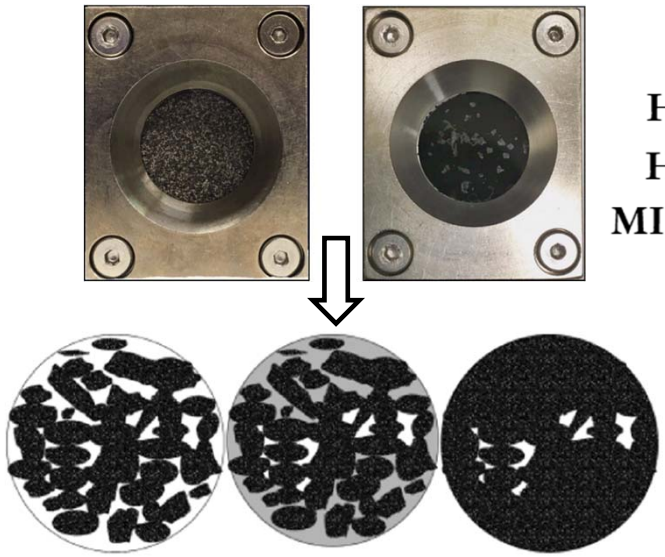

d-H_2O
d-decane
d-THF

Porosity Results(%)

mudrock	Sample 1	Sample 2	Sample 3
Total	11.4	7.83	9.28
Hydrophyllic	7.04	2.7	7.16
Hydrophobic	4.92	2.58	2.32
MICP Accessible	2.12	0.79	3.71

- Yang et al., Fuel, 2017
- Sun et al., IJCG, 2017
- Zhao et al, SR, 2017
- Zhang et al., MPG, 2019

Summary

- Multiple and complementary approaches are developed for pore structure and fluid movement studies
- Different pore structure characteristics, especially pore connectivity, is observed for reservoir and source rocks
- Microscopic pore connections influence macroscopic fluid flow and hydrocarbon movement

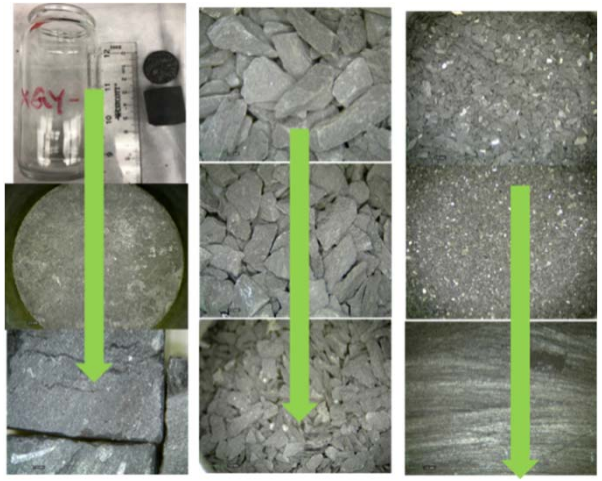

Acknowledgments

UNIVERSITY OF TEXAS–ARLINGTON

RPSEA Research Partnership to Secure Energy for America

ConocoPhillips

Sinopec

Oak Ridge National Laboratory

CNPC 中国石油

NEUP Nuclear Energy University Program

U.S. Department of Energy

NIST

USGS science for a changing world

Bureau of Economic Geology

O.D.N.R. Geological Survey

Pennsylvania Geological Survey Est. 1836

North Dakota Geological Survey 1895

New Mexico Bureau of Geology and Mineral Resources — New Mexico Tech — Earth Science for the 21st Century

Vitruvian Exploration

element petroleum III, llc

Diamondback Energy

Pioneer Natural Resources

Exxon XTO Energy